CR 73230

AVAILABLE TO THE PUBLIC

INTERIM REPORT
CONTRACT NAS 2—3427

MATERIAL PROPERTIES MEASUREMENTS FOR SELECTED MATERIALS

By

A. H. Jones
W. M. Isbell
F. H. Shipman
R. D. Perkins
S. J. Green
C. J. Maiden

Prepared for

NATIONAL AERONAUTICS AND SPACE ADMINISTRATION
AMES RESEARCH CENTER, MOFFETT FIELD
CALIFORNIA 94035

MATERIALS & STRUCTURES LABORATORY
MANUFACTURING DEVELOPMENT
GENERAL MOTORS CORPORATION
GENERAL MOTORS TECHNICAL CENTER, Warren, Michigan 48090

MSL-68-9

APRIL, 1968

COPY NO. 2

INTERIM REPORT
CONTRACT NAS2-3427

MATERIAL PROPERTIES MEASUREMENTS FOR SELECTED MATERIALS

By

A. H. Jones
W. M. Isbell
F. H. Shipman
R. D. Perkins
S. J. Green
C. J. Maiden

Prepared for

NATIONAL AERONAUTICS AND SPACE ADMINISTRATION
AMES RESEARCH CENTER, MOFFETT FIELD
CALIFORNIA 94035

MATERIALS & STRUCTURES LABORATORY
MANUFACTURING DEVELOPMENT
GENERAL MOTORS CORPORATION
GENERAL MOTORS TECHNICAL CENTER, Warren, Michigan 48090

MSL-68-9

APRIL, 1968

ABSTRACT

Hugoniot equation of state measurements were made on Coconino sandstone, Vacaville basalt, Kaibab limestone, Mono Crater pumice and Zelux (a polycarbonate resin) for pressures to 2 Mb. A single data point was obtained for fused quartz at 1.6 Mb.

In addition to the hugoniot studies, the uniaxial compressive stress behavior of Vacaville basalt and Zelux was investigated at strain rates from about 10^{-5}/sec to 10^{3}/second. The data presented include the stress-strain relations as a function of strain rate for these two materials.

(Page ii is blank)

TABLE OF CONTENTS

LIST OF ILLUSTRATIONS

[redacted]

LIST OF TABLES

(Page vi is blank)

SECTION I

INTRODUCTION

The behavior of materials under the action of shock wave loadings has been under intensive investigation during the past decade.(1) Some have been concerned with geophysically oriented investigations of crustal rocks and possible earth core materials. Another area of concentrated research concerns the effect of hypervelocity meteorite impact on crustal rocks.

In order to understand the complex phenomena occurring in and around a forming impact crater, it is necessary to have knowledge of the characteristics of the material over a wide range of stresses since the impact induced shock wave attenuates rapidly as it propagates away from the point of origin. The shock wave may originally have an amplitude of many megabars but is attenuated by rarefactions arising due to the finite size of the impacting body, the divergence of the wave front and by energy absorbing mechanisms within the medium. One such mechanism is that of polymorphism of the crystalline constituent. Another loss process occurs during the comminution of the rock.

This report describes experiments in which data was acquired for several selected geological materials in the high pressure region and the elastic to fracture region of stress. Hugoniot equations of state in the pressure range 0.03 to 2 Mb have been determined for Coconino sandstone, Kaibab limestone, Vacaville basalt, and Mono Crater pumice. Also, a single hugoniot data point for fused quartz was obtained at 1.6 Mb. The high intensity shock wave studies are described in Section II, Measurement of Shock Wave Parameters. The experimental technique is described and the results are presented.

The compressive behavior of basalt in uniaxial stress over a range of strain rates from approximately 10^{-5}/sec to 10^{3}/sec was examined to provide basic data describing the behavior of this material. The experimental techniques and the results obtained are described in Section III, High Strain-Rate Studies.

An additional non-geological material, Zelux, a stress-relieved polycarbonate resin having a high impact strength, was studied. Both the high pressure hugoniot and the strain-rate behavior of the materials were experimentally determined, and the results are reported in the appropriate sections.

SECTION II

MEASUREMENT OF SHOCK WAVE PARAMETERS

EXPERIMENTAL TECHNIQUE

To induce multi-megabar pressures in specimen materials, flat plates of high shock impedance are accelerated by a light gas gun to velocities extending above 8 km/sec. The plates are made to impact an instrumented specimen and induce a shock wave with the initiating conditions accurately controlled and recorded. Several time-related measurements may be made of shock wave phenomena and then used to partially describe the thermodynamic state of the specimen material at very high pressures.

The gun used to accelerate the impactor is an accelerated-reservoir light gas gun(2) with a launch tube bore diameter of either 29 mm or 64 mm. This type of gun maintains a reasonably constant pressure at the base of the projectile during the launch allowing the acceleration of a variety of unshocked impactor materials to study shock wave phenomena at high pressures.

Figure 1 shows the layout of the range. The gun consists of the following major components:

1. Powder chamber.
2. Pump tube, 89 mm internal diameter by 12 m long.
3. Accelerated-reservoir high-pressure coupling.
4. Launch tube, either 29 mm internal diameter by 8 m long or 64 mm diameter and 8 m long.
5. Instrumented target chamber and flight range.

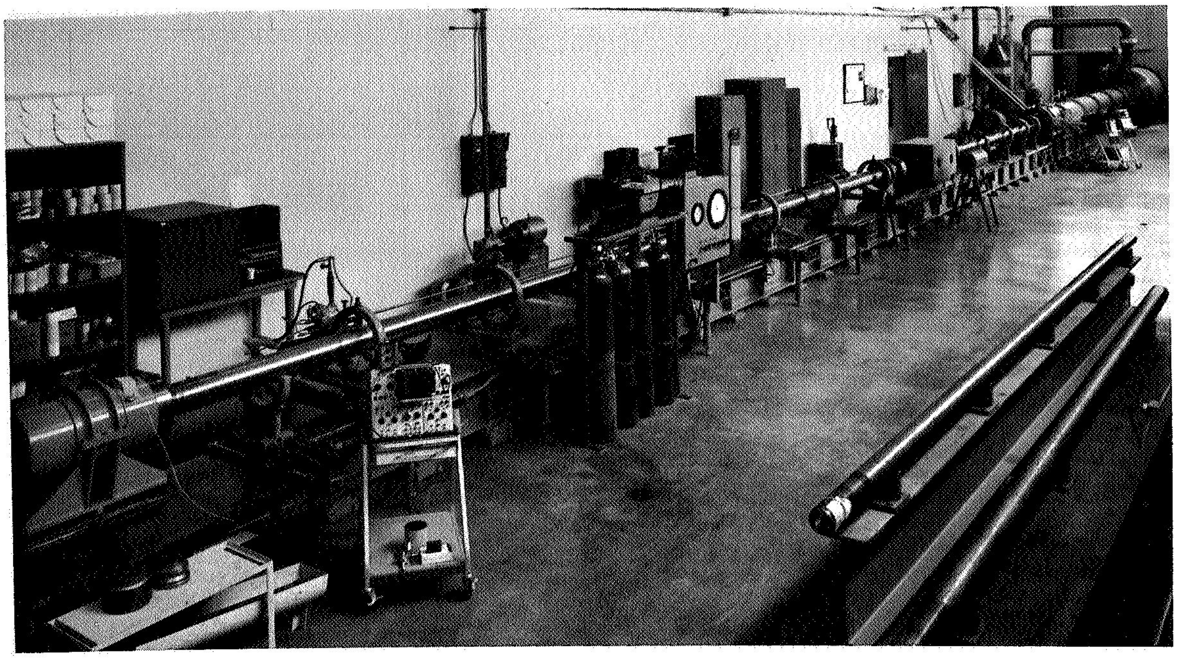

Figure 1   Layout of ARLG Gun Range

When the gun is loaded for firing, gunpowder is placed in the powder chamber and the pump tube is filled with hydrogen. The hydrogen is compressed by a plastic nosed piston which has been accelerated by the burnt gunpowder. In turn, the projectile is accelerated by the release of the compressed hydrogen through a high pressure burst diaphragm.

Prior to firing, the flight range and instrument chamber are evacuated and then flushed with helium to approximately 10^{-6} Torr to eliminate any spurious effects due to gas build-up and ionization between projectile and target. The sealing lips on the rear of the plastic sabot are pressed tightly against the sides of the launch tube by the high pressure gas and effectively eliminate blow-by of the hydrogen gas.

Careful attention to the condition of the launch tube is necessary for successful firing in the high velocity ranges. Bore linearity of better than 0.2 mm over the full 8 m length of the launch tube is maintained. The internal diameter is maintained to within 0.01 mm. Launch tubes are cleaned and honed after each firing and are removed every 15 to 20 firings for reconditioning.

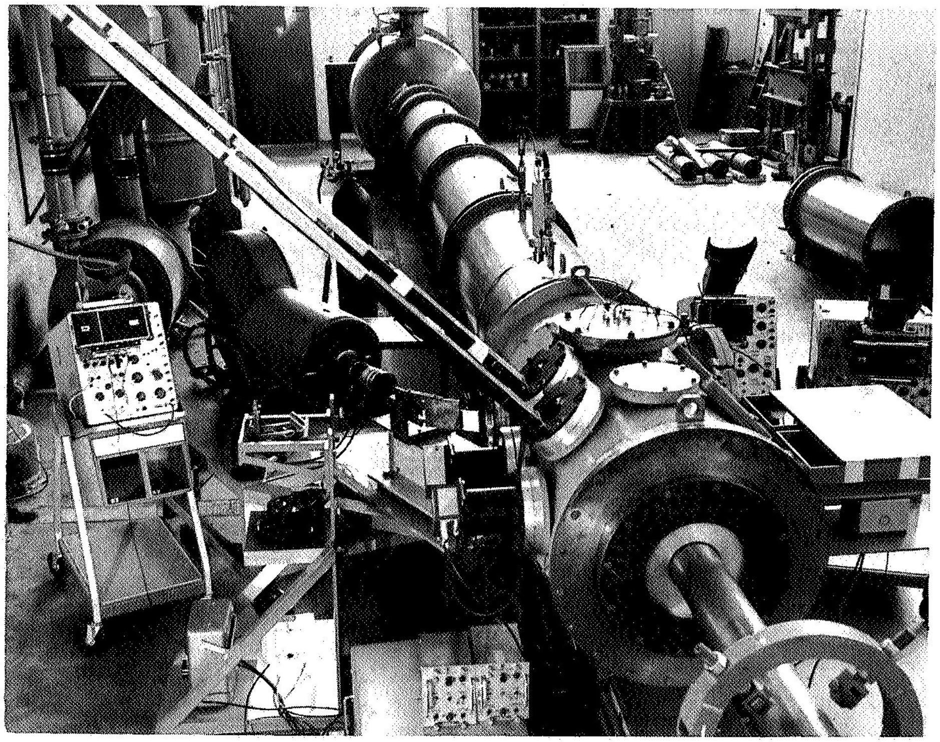

Figure 2 Target Chamber Set-up, with Continuous-Writing Streak Camera in Position

Figures 2 and 3 show the instrumentation chamber designed for the high pressure studies. This chamber is connected to the barrel of the gun through an O-ring seal to allow free axial movement of the launch tube. The target chamber and target are shock-mounted to prevent premature motion before projectile impact. To facilitate this, several stages of mechanical isolation have been arranged in the barrel, I-beam support structure and concrete foundation.

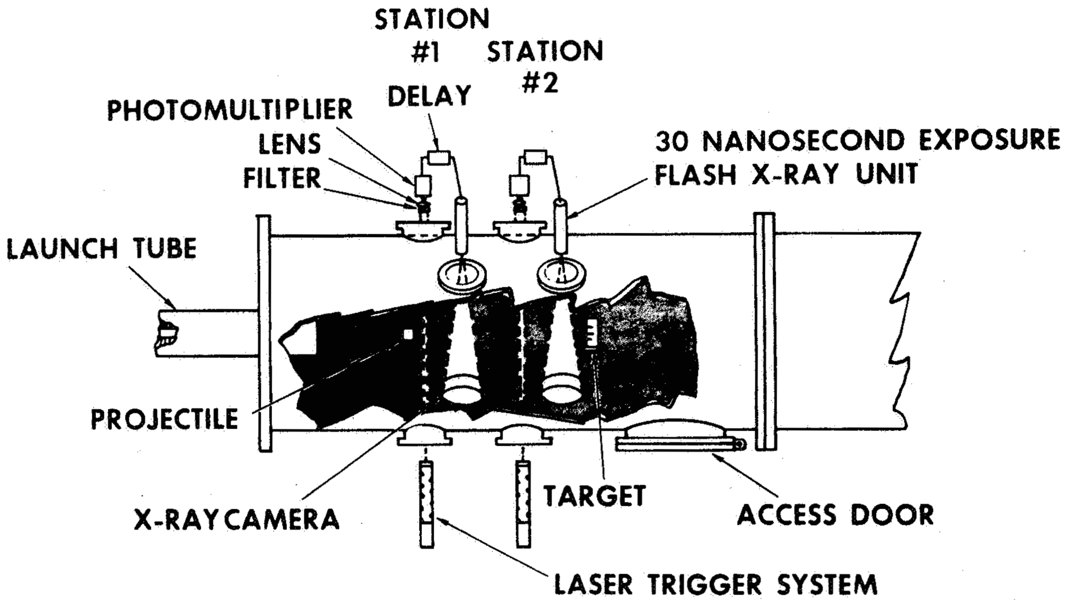

Figure 3 Top Cutaway View of Target Chamber

The impact chamber is a steel cylinder of 61 cm O.D. and 1.5 m length. Physical access and instrument ports are precisely machined in a horizontal plane and in planes 45° above horizontal. Two stations of six ports each are accurately spaced 30.5 cm apart.

Operationally, the ports are closed against O-ring vacuum seals with Plexiglas or magnesium windows for optical and x-ray access or with steel cover plates.

The impactor velocity measuring system consists of a laser triggering system and two short duration flash x-rays. With this system, impactor velocities are measured accurate to 0.2%. The triggering system consists of a neon-helium gas laser aimed at a photo-detector across the impact chamber orthogonal to and intersecting the line of flight of the projectile. A photomultiplier monitors the laser light output through a set of masks and a narrow band filter. When light interruption occurs due to projectile passage, a sharp change of voltage level is converted into a trigger signal of sufficient voltage to initiate a Field Emission Corporation 30 nsec dual flash x-ray unit. The x-ray flash exposes a polaroid film plate on the opposite side of the chamber by means of a fluorescing intensifier screen. The trigger and x-ray flash system is then duplicated to record the passage of the projectile in the second field to view 30.5 cm further down range.

The spacing between the two x-ray field centerlines is indicated by fiducial wires which are measured by an optical comparator to within 0.02 mm. Measurements of the impactor face position relative to the window fiducials allow calculation of actual projectile position and travel over the time interval measured between flash exposures. Figure 4 is an example of the shadowgraphs of the two x-ray stations showing the projectile in free flight before impact.

A second method is also employed to measure impactor velocity. The time interval between the first x-ray flash and the event of closure of a rear surface shock velocity pin is recorded. The impactor and target positions are measured from the x-ray shadowgraphs and a velocity is calculated. Variations in measurements between the two techniques are usually less than 0.05%.

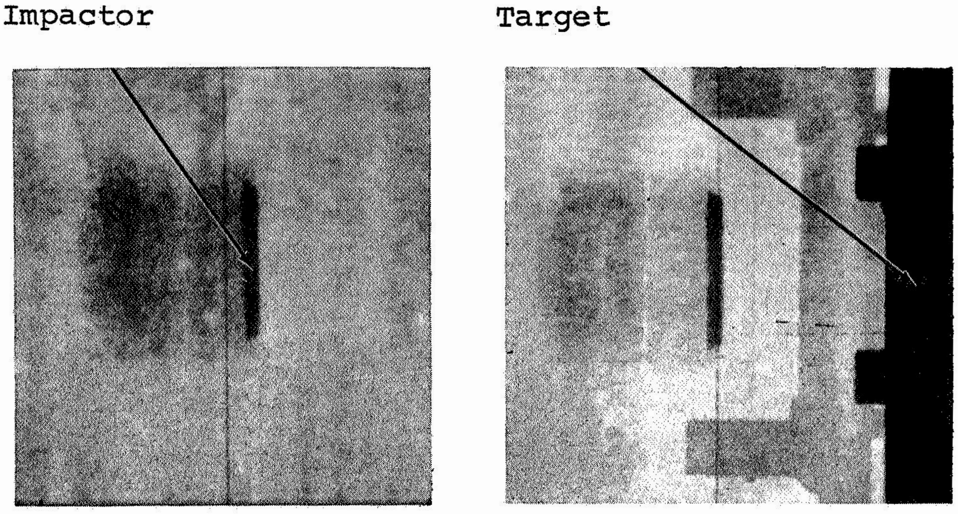

Station #1

Station #2

Figure 4 X-ray Shadowgraphs of Projectile Before Impact

The target is located approximately 60 cm from the launch tube muzzle and is included in the #2 x-ray field of view. Measurements of the shock wave transit time in the target are made using four coaxial self-shorting pins as sensors. The shorting of a pin results in a sharply rising current to ground which produces a signal across the time-interval-meter input termination resistors. The circuit is so designed that each pin signal can be seen on three output lines and is free of any reflections or ringing for several hundred nanoseconds. The individual circuits are "tuned" by the use of trimmer capacitors so that the rise time of each signal is 1.0 ± 0.1 nsec to 12 volts. Thus it is possible for the combined mechanical-electronic signal system to make use of the ± 1/2 nsec resolution of the time recording instruments.

The shock wave transit time-interval-meters are Eldorado Models 793. These counters have a specified time resolution of ± 1/2 nsec and may be read digitally to the nearest nanosecond. They require an input signal of 1 volt with a rise time approximately 1 nsec. Although instrument stability is specified to be one part in 10^4 for long term and five parts in 10^6 for short term, in actual practice, the instruments are calibrated prior to each shot over a period of about 30 minutes. The shot is then fired within five minutes of completion of the calibration procedure.

The impactor striking tilt time interval is recorded on Polaroid film from a Tektronix 519 oscilloscope trace. The sweep rate employed is 20 nsec/cm but is nonlinear in the first centimeter. A calibration plot is periodically generated and is used to correct the recorded time interval.

The planarity of the shock wave induced in the target is dependent on the impactor flatness at impact. The impactor surface is machine lapped and then hand polished flat to 0.5×10^{-3} mm. Tests performed with impactors of Fansteel-77 and OFHC copper indicate the surface curvature after launch to be less than 1 nsec at a launch velocity of 7 km/sec.

The impactor tilt relative to the target specimen front surface is sensitive to launch tube linearity and sabot alignment as well as on target alignment even though the projectile flies free from the launch tube before impact. The capability to adjust the target position and perpendicularity relative to the launch tube centerline by an optical technique brings the average tilt at impact to approximately 0.03 radians.

Because of the comparatively gentle acceleration of the projectile to its terminal velocity, the impactor plate is not shock heated. In addition, free flight in an evacuated range precludes aerodynamic heating. This accounts for the flatness of the impactor after launch and significantly reduces the complexity of the experiment. The estimated temperature rise during launch is of the order of 1°C.

TARGET SYSTEM AND SPECIMEN PREPARATION

The basic features of the target are as shown in Figure 5. Two pins are passed by the ends of the specimen block even with the specimen front surface. These pins are used to measure impactor tilt in terms of the time interval of their respective closures; therefore, their cap faces must lie in the same plane as the target impactor surface. Two more pins are spring loaded in place at the rear surface of the target and on a line joining the two tilt pints. Thus two measurements of shock transit time are made for each firing.

The coaxial self-shorting pins* consist of an outer sheath of brass surrounding a teflon sleeve and a copper inner conductor. The pins are connected to electrical cables by soldered joints and are made self-shorting, i.e., the target specimen does not have to be a conductor, by the placement of a cap over the sensing end which leaves a small gap (on the order of 0.050 ± .002 mm) between it and the end of the inner conductor. The pin gaps are measured by x-ray shadowgraphy and the measurements are used as corrections in the shock velocity calculations as pin closure times.

---

* Model CA-1039, Edgerton, Germeshausen and Grier, Santa Barbara, California.

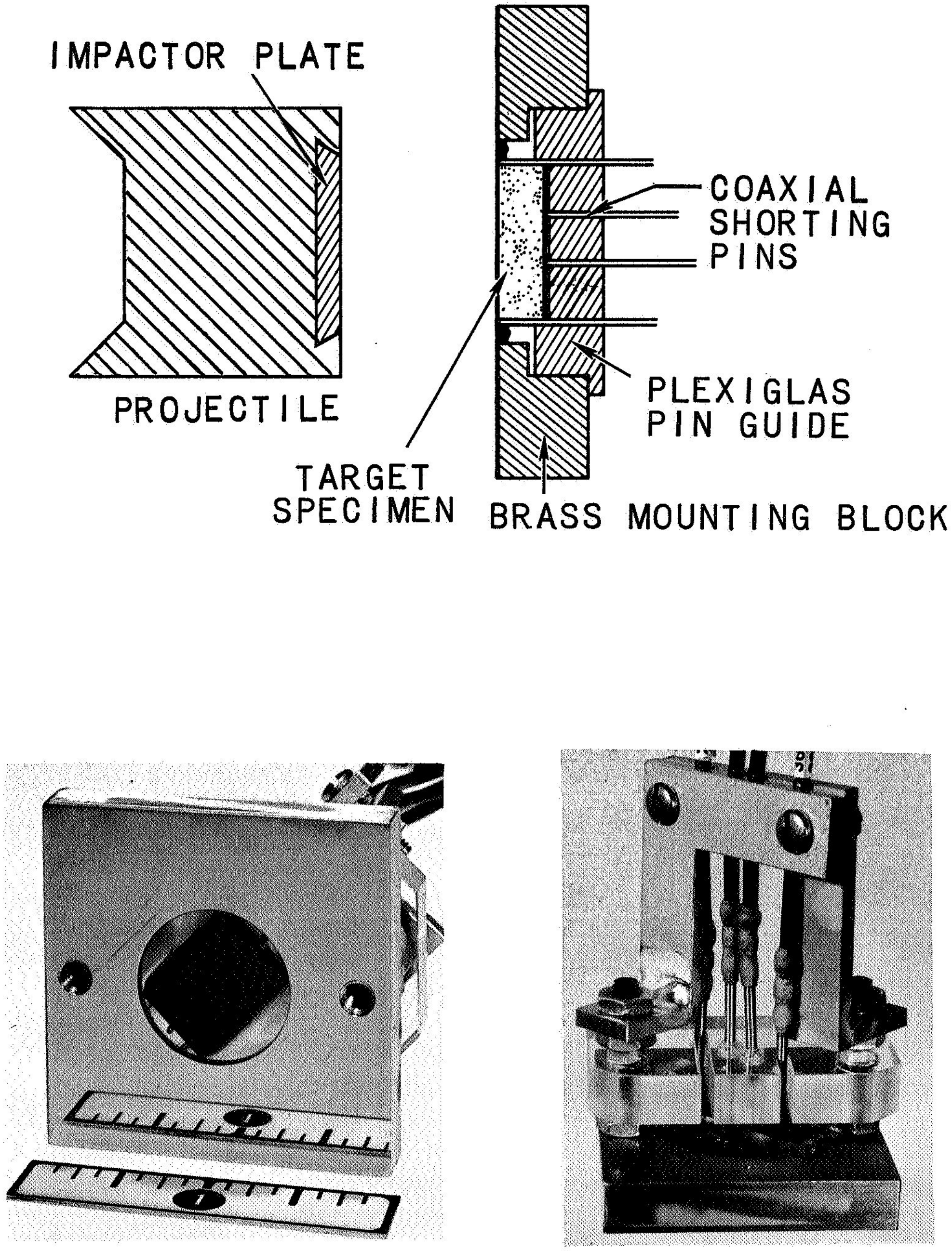

Figure 5 Equation of State Studies Target Configuration

Because rarefactions originate at the free surfaces of the specimen block, the targets are designed so that the pin locations are inside the unrarefacted region at the target rear surface. Projectile and target thickness are so chosen to insure against premature attenuation of the shock wave from the rarefaction waves originating at the impactor rear surface.

The target specimens were cut from the parent material and ground to final dimensions. The targets were ground under a high sluicing flow to prevent local heating and chipping. The basalt and dolomite target surfaces, front and rear, were machine and hand lapped flat and parallel to within 10^{-3} mm. The procedures used for sandstone and pumice differed from those used in preparing the basalt and dolomite in that lapping and polishing were impossible due to the high porosity and irregular surfaces.

The target specimen thicknesses were measured with a Zeiss light-section microscope, which avoids the problem of an indicator marring the specimen surfaces and also simplified the measurement of irregular surfaces such as found on the porous materials.

The porous materials required several changes from standard target construction. The highest points of surface, as measured with the microscope, were taken as the surface plane. A 0.1 mm thick copper shim was then placed on the upper surface of the specimens against which the spring loaded shorting pins were set. The effect of this thin shim on the measurement of the shock wave transit time was corrected for in the shot analysis.

A viscous quick-setting epoxy was employed to mount the porous specimens in the brass mounting block, avoiding the problem of the potting epoxy soaking into the specimen. Microscopic examination showed no intergranular seepage of Epon 911 in neither sandstone nor pumice even though Hysol Epoxy-Patch penetrated 1 mm in sandstone and ~ 4 mm in pumice.

The highest pressure hugoniot points were obtained using a small target specimen and a small impactor, the reduced weight of the projectile allowing achievement of a higher launch velocity. The high pressure target design, used only for the basalt, Coconino sandstone, fused quartz and Zelux, were similar to the targets described previously, except that a 1 cm diameter specimen was used and only one shorting pin was placed on the rear surface instead of two.

EQUATION OF STATE MEASUREMENTS

Consider the sudden application of a high stress, such as the impact of a high velocity plate, to the plane surface of a material. The description of the ensuing flow conditions can be found using the conservation relations for mass, momentum and energy:

$$\rho_o U_s = \rho_1 (U_s - u_{p1}) \qquad \text{Conservation of mass} \quad (1)$$

$$P_1 - P_o = \rho_o U_s u_{p1} \qquad \text{Conservation of momentum} \quad (2)$$

$$E_1 - E_o = 1/2(V_o - V_1)(P_1 - P_o) \qquad \text{Conservation of energy} \quad (3)$$

where subscripts o and 1 denote conditions ahead of and behind the advancing shock front respectively. The terms are: U_s = shock velocity, u_p = particle velocity, P = shock stress, ρ = density, $V = 1/\rho$ = specific volume and E = specific internal energy. All velocities are determined with respect to a stationary observer.

The experimental determination of U_s and v = impact velocity, along with knowledge of the initial conditions, ρ_o, P_o and E_o allows the calculation of the shock stress, P_1; volume, V_1 and internal energy, E_1.

Each set of determinations allows the calculation of a single point on the locus of shock states achievable from the same initial material conditions. The locus of shock states then defines the hugoniot of the material and may be determined experimentally by applying different incoming stresses (different impact velocities and/or different shock impedance impactor materials).

The indirect approach generally taken for the determination of the particle velocity, u_p, is referred to as an impedance match technique.(3) The impedance match technique requires knowledge of the hugoniot of the impactor material. The shock impedance of a material is given by $\rho_o U_s$ (which is the slope of a line originating at $P = 0$, $u_p = 0$). The measurement of the impactor velocity establishes the origin of the impactor hugoniot. The intersection of the impedance line with the reflected hugoniot of the impactor establishes the shock stress and specimen particle velocity. Analytically this is given by:

$$B = \rho_{oi} C_{oi} + \rho_{ot} U_s + 2 \rho_{oi} S_i \, v$$

$$u_p = \frac{B - \sqrt{B^2 - 4 \rho_{oi}{}^2 \, S_i \, v (C_{oi} + S_i \, v)}}{2 \rho_{oi} S_i} \tag{4}$$

where the linear equation:

$$U_s = C_{oi} + S_i u_{pi} \tag{5}$$

$$u_{pi} = (v - u_p) \tag{6}$$

serves to describe the impactor material behavior in the $U_s - u_p$ plane. Subscripts $\underline{i}$ and $\underline{t}$ refer to impactor and target respectively. The shock stress is found by substitution into Equation (2) (P_o is assumed equal to zero).

HUGONIOT OF THE IMPACTOR MATERIALS

To perform the impedance match solution described above, it is necessary to have previously determined the hugoniot of the impactor plate. Two materials were used as impactors for this project; OFHC copper was used for experiments in which low and intermediate pressures were to be induced in the specimen and Fansteel-77, a tungsten alloy, was used to generate the very high pressures. Hugoniot measurements were made on these materials by impacting specimens of the material with impactors of the same material over a wide range of impact velocities. Measurements were made of the shock velocity of the induced wave and of the velocity of the impactor. Particle velocity behind the shock wave was calculated by assuming conditions of symmetrical impact, i.e., particle velocity equals one-half impact velocity.

The constants thus obtained for the two materials and subsequently used to analyze the experiments on geological materials are shown below:

OFHC Copper:

$$U_s = 3.96 + 1.497\ u_p \text{ km/sec}, \quad \rho_o = 8.93 \text{ gm/cm}^3$$

Fansteel-77: (90% W, 6% Ni, 4% Cu)

$$U_s = 3.96 + 1.295\ u_p \text{ km/sec}, \quad \rho_o = 17.01 \text{ gm/cm}^3$$

EXPERIMENTAL RESULTS

The experimentally determined hugoniot data for Vacaville basalt, Kaibab limestone, Coconino sandstone, fused quartz, Mono Crater pumice and Zelux are presented and discussed in this section. The physical properties and experimental data are presented in tabular form and the shock wave data are displayed graphically to facilitate discussion and comparison with other work. The experimental errors are displayed only in the U_s-u_p plane but are numerically expressed in the tables. Summary of results is given in Table XI at the end of the present section.

Vacaville Basalt

Figure 6 displays the hugoniot data determined in this program for Vacaville basalt over a pressure range of 0.35 to 2.05 Mb. The descriptive physical data are presented in Table I. The composition of Vacaville basalt is identical to that of the material tested by Ahrens(4) except for a slightly higher initial density (i.e. 2.86 vs. 2.82 gm/cm^3). The lower pressure data published by Ahrens is shown in Figures 7a and 7b and suggests a hugoniot elastic limit of about 0.050 Mb, at a wave velocity of 5.35 km/sec.

The hugoniot data are presented in Table II. One test was performed with a pressure in the double-shock wave region. Since the present pin technique records only the arrival of the precursor wave, it is not surprising that the measured shock velocity was 5.34 ± 0.06 km/sec - virtually the elastic wave velocity. This shot is included in Figure 6 in parentheses since the true particle velocity associated with the wave cannot be determined. The other experiments presented here are all at pressures higher than the limit of the 0.3 Mb double wave region as determined by Ahrens, allowing the impedence match method to be applied for the determination

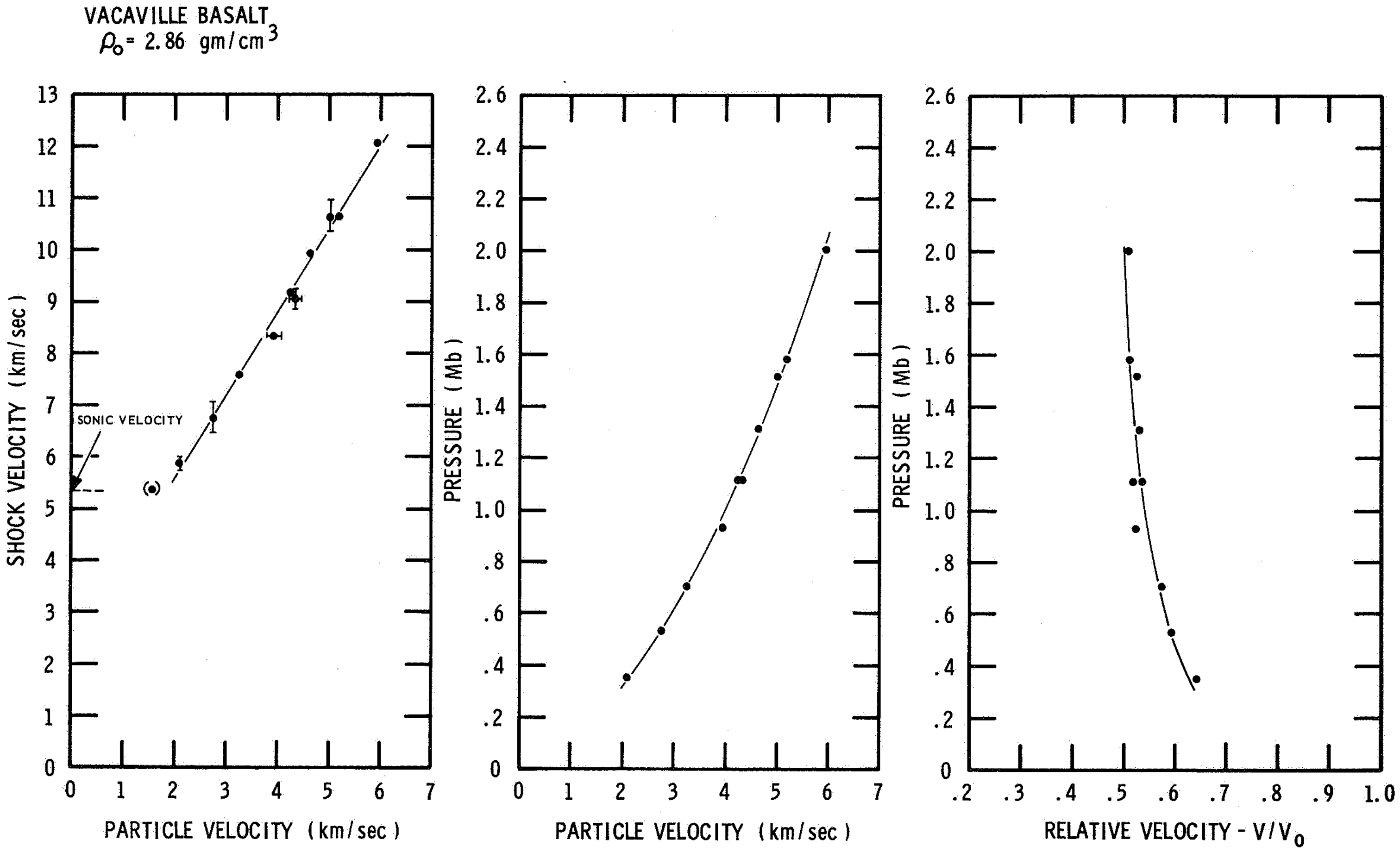

Figure 6 Hugoniot Data for Vacaville Basalt

TABLE I

PHYSICAL PROPERTIES OF VACAVILLE BASALT*

Mineral Composition

53%	Plagioclase Feldspar
31%	Augite
9%	Magnetite & Ilmenite
5%	Celadonite **
2%	Apatite

Grain Size

Modal Grain Size = 0.08 mm
Range Grain Size = 0.3 - 0.003 mm

Density = 2.89 gm/cm^3

Chemical Composition

SiO_2	50.3%
Al_2O_3	13.8%
Fe_2O_3	3.5%
FeO	9.1%
MgO	4.4%
CaO	7.7%
Na_2O	3.3%
K_2O	1.6%
H_2O^-	1.0%
H_2O^+	1.5%
TiO_2	2.4%
P_2O_5	1.2%
MnO	.24%
CO_2	.05%

Strength

Average Compressive Strength = 2.56×10^9 dynes/cm^2
(block size 2.2 x 2.2 x 4.5 cm)

Range in Compressive Strength = $1.56 \times 10^9 - 3.69 \times 10^9$ dynes/cm^2

Average Shear Strength (calc) = 8.6×10^8 dynes/cm^2

Average Tensile Strength = 1.42×10^8 dynes/cm^2
(rod size 1.1 x 1.1 x 1.5 cm)

Range in Tensile Strength = $0.90 \times 10^8 - 2.32 \times 10^8$ dynes/cm^2

* The tables of physical properties were provided by D. E. Gault, private communication.

** Microscopic examination.

TABLE II

HUGONIOT DATA FOR VACAVILLE BASALT

$\rho_o = 2.86$ gm/cm^3

U_s Shock Velocity (km/sec)	U_p Particle Velocity (km/sec)	P Pressure (Megabar)	V/V_o Relative Volume
5.34 ± .06	(1.59)^x		
5.88 ± .15	2.10	.353 ± .009	.643 ± .009
6.77 ± .28	2.76	.534 ± .022	.592 ± .017
7.59 ± .05	3.24	.703 ± .005	.573 ± .003
8.31 ± .06	3.94 ± .12*	.936 ± .035	.526 ± .018
9.19 ± .05	4.25	1.117 ± .006	.538 ± .002
9.01 ± .18	4.33 ± .12*	1.116 ± .052	.520 ± .022
9.91 ± .07	4.64	1.315 ± .009	.532 ± .003
10.60 ± .27	5.01	1.519 ± .039	.529 ± .010
10.63$^+$	5.20	1.581	.511
12.04$^+$	5.94	2.046	.507

x Impedence match method not applicable

* Estimated Impact Velocity

\+ Single Pin Value

of particle velocity and pressure. Several shots were fired at nearly the same impact velocity to check test reproducibility. The scatter in the individual data points is somewhat larger than expected for such a fine-grained, homogeneous material, and may in part be attributable to the difficulties experienced in calibrating the time interval counters used for measurement of shock wave velocity during this early part of the program. The linear fit through the hugoniot state points in the $U_s - u_p$ plane is given by:

$$U_s = 2.31 + 1.615\, u_p \text{ km/sec}$$

$$\text{Sigma } U_s = \pm\, 0.20 \text{ km/sec}$$

The lower pressure data of Ahrens,(4) Bass,(5) and L.R.L.(6) are included in Figure 7 to illustrate the similarities in the basalts tested. The Vacaville basalt of Ahrens exhibited a two-wave structure, as witnessed by optical techniques up to the highest pressure obtained by him, i.e. ~0.2 Mb. Unfortunately, there is no overlap with the present work which would allow direct comparison. It is seen that the data of Bass and L.R.L. for the Nevada Test Site basalt agrees within experimental accuracy with the present as well as Ahrens' data, despite the lower density of their basalt (2.67 gm/cm^3).

Kaibab Limestone

The hugoniot for Kaibab limestone, which is an alpha member dolomite, was determined over a pressure range of 0.3 to 1.13 Mb. The approximate mineral analysis and physical description given in Table III shows the limestone to be approximately 75% dolomite, 20% quartz and 5% calcite, feldspar, etc. Porosity is 20 - 24%. The hugoniot results are listed in Table IV and are shown in Figure 8.

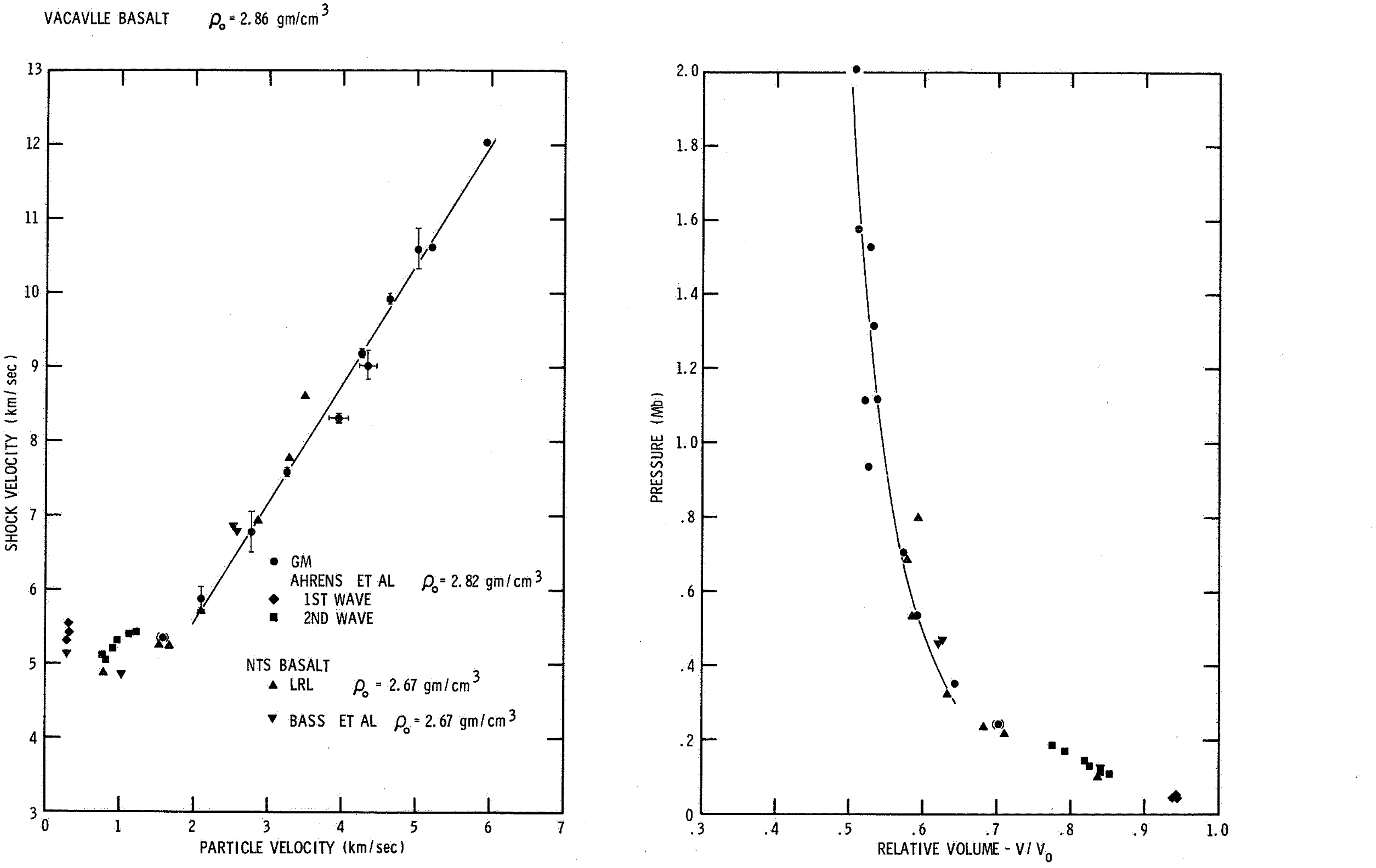

7a

7b

Figure 7 Comparison of Hugoniot Data for Vacaville Basalt with Hugoniot Data of Other Basalts

TABLE III

PHYSICAL PROPERTIES OF KAIBAB LIMESTONE (ALPHA MEMBER) DOLOMITE

Mineral Analysis

75%	Dolomite
20%	Quartz
5%	Calcite, Feldspar, Clay Minerals, Hematite, Goethite, Heavy Minerals

Density

Bulk Density - 2.12 - 2.22 gm/cm^3

Grain Density = 2.79 gm/cm^3

Porosity	Acoustic Velocity
20.3 - 23.8%	2.845 km/sec

Strength

Unconfined Crushing Strength

(block size 2.2 x 2.2 x 4.5 cm = 3.50 - 4.30 x 10^8 dynes/cm^2)

TABLE IV

HUGONIOT DATA FOR KAIBAB LIMESTONE

$\rho_o = 2.22 \text{ gm/cm}^3$

U_s Shock Velocity (km/sec)	U_p Particle Velocity (km/sec)	P Pressure (Megabar)	V/V_o Relative Volume
5.69 ± .05	2.35	.297 ± .003	.587 ± .004
6.96 ± .15	3.20	.494 ± .011	.541 ± .009
8.65 ± .15	4.23	.812 ± .014	.511 ± .008
9.22 ± .06	4.69	.961 ± .011	.491 ± .004
10.10 ± .17	5.05 ± .24*	1.131 ± .055	.500 ± .033

* Estimated Impact Velocity

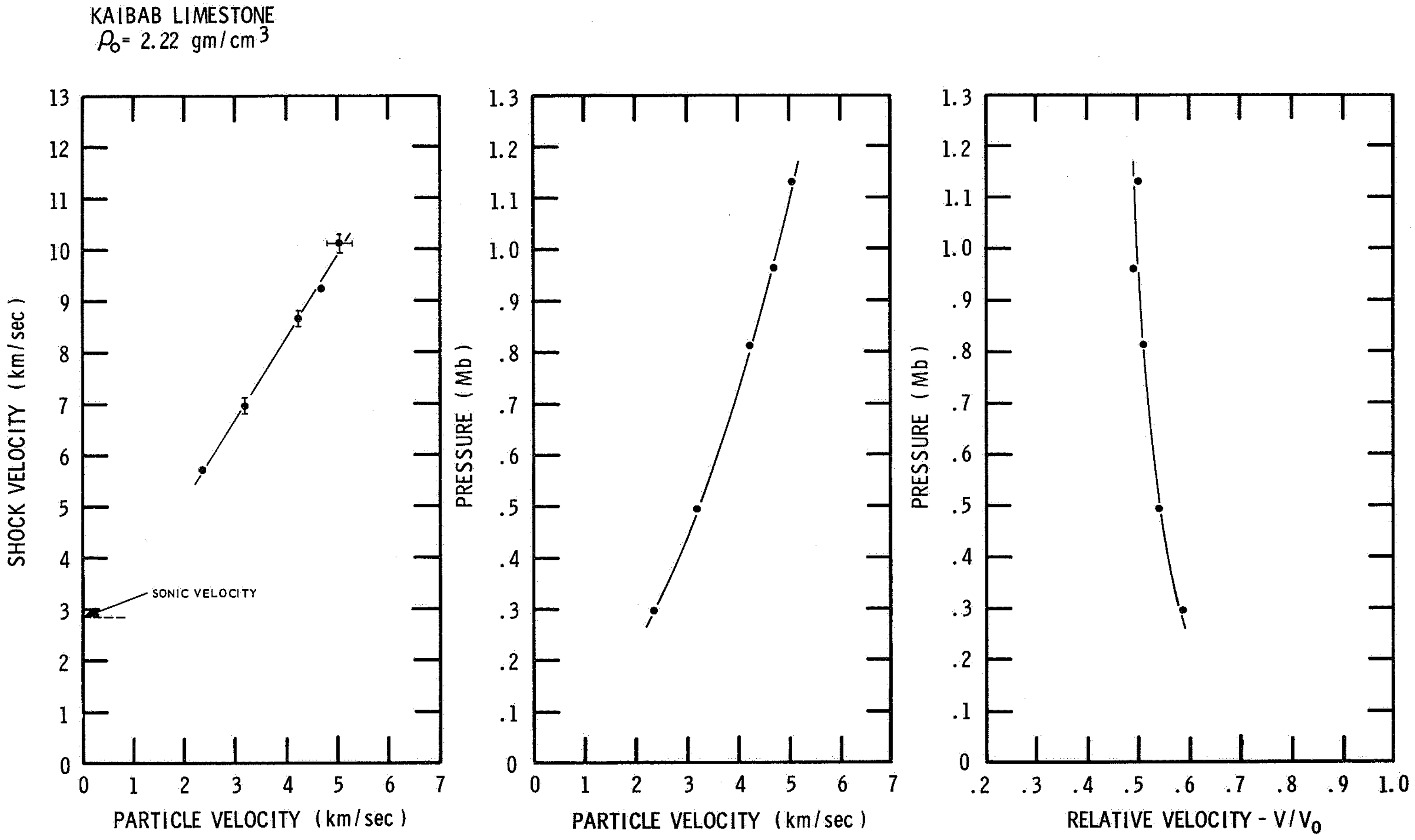

Figure 8 Hugoniot Data for Kaibab Limestone

The linear fit to the experimentally determined hugoniot points is given by

$$U_s = 1.89 + 1.597\, u_p \quad \text{km/sec}$$

$$\text{Sigma } U_s = \pm\, 0.13 \quad \text{km/sec}$$

Coconino Sandstone

The Coconino sandstone, a highly pure polycrystalline quartz weakly cemented with silica, was tested over the pressure range of 0.2 to 1.2 Mb. The physical properties are shown in Table V. Figure 9 presents the hugoniot data graphically and Table VI lists the numerical values obtained by these tests. The porosity of the Coconino sandstone caused some target preparation and assembly problems, although the data obtained from each test showed surprisingly little scatter.

Included in Figure 9 is the linear fit reported by Ahrens for data obtained by him for pressures to 0.2 Mb. A better means for making comparison is shown in the pressure specific volume plot in Figure 10. The hugoniot for the Coconino sandstone can be conveniently divided into five regions. The initial region (not shown in Figure 10) is the elastic region. The second region is primarily the crushing of the sandstone to the volume of the single-crystal quartz which is seen to be achieved at approximately 0.025 Mb. In region three, from 0.025 Mb to around 0.07 Mb, the hugoniot follows closely the hugoniot of solid quartz. Above this pressure it can be seen that the specific volumes achieved by the shocked sandstone are less than those achieved by quartz upon isothermal compression. For this reason we conclude that the quartz has been transformed into a higher density form of silica. This in turn is followed by another phase

TABLE V

PHYSICAL PROPERTIES OF COCONINO SANDSTONE

Mineral Composition

97%	Quartz
3%	Feldspar
Trace	Clay and Heavy Minerals

Grain Size

Average and Modal Grain Size = 0.117 - 0.149 mm
Range with Grain Thickness 0.062 - 0.71 mm

Density

Bulk Density = 1.98 gm/cm^3
Grain Density = 2.67 gm/cm^3

Porosity (calc)

25.8%

Strength

Unconfined Crushing Strength normal to bedding
3.14×10^8 $dynes/cm^2$ dry, 3.64×10^8 $dynes/cm^2$ saturated H_2O
(block size 2.2 x 2.2 x 5 cm)

Description

Sandstone is weakly to moderately well cemented with silica, in the form of quartz overgrowths on the grains. Subparallel laminae 5.0 to 17.5 mm thick are separated by thin laminae 0.5 mm thick containing more than average amounts of silt and clay sized grains.

TABLE VI

HUGONIOT DATA FOR COCONINO SANDSTONE AND FUZED QUARTZ

Coconino Sandstone $\rho_o = 1.98$ gm/cm^3

U_s Shock Velocity (km/sec)	U_p Particle Velocity (km/sec)	P Pressure (Megabar)	V/V_o Relative Volume
3.674 ± .001	1.33	.097	.637 ± .001
4.10+	1.63	.132	.602
4.49 ± .10	2.18	.194 ± .004	.514 ± .011
4.84 ± .02	2.57	.256 ± .001	.468 ± .002
5.66 ± .01	3.12	.349 ± .001	.449 ± .001
5.79 ± .04	3.25	.373 ± .002	.438 ± .005
7.57 ± .03	4.30	.644 ± .003	.432 ± .002
7.79 ± .14	4.43	.684 ± .011	.431 ± .010
8.82 ± .03	5.07	.886 ± .003	.425 ± .003
10.09+	5.94	1.186	.411
11.20+	6.43	1.426	.426

Fused Quartz $\rho_o = 2.204$ gm/cm^3

11.42+	6.34	1.596	.445

* Estimated Impact Velocity

\+ Single Pin Value

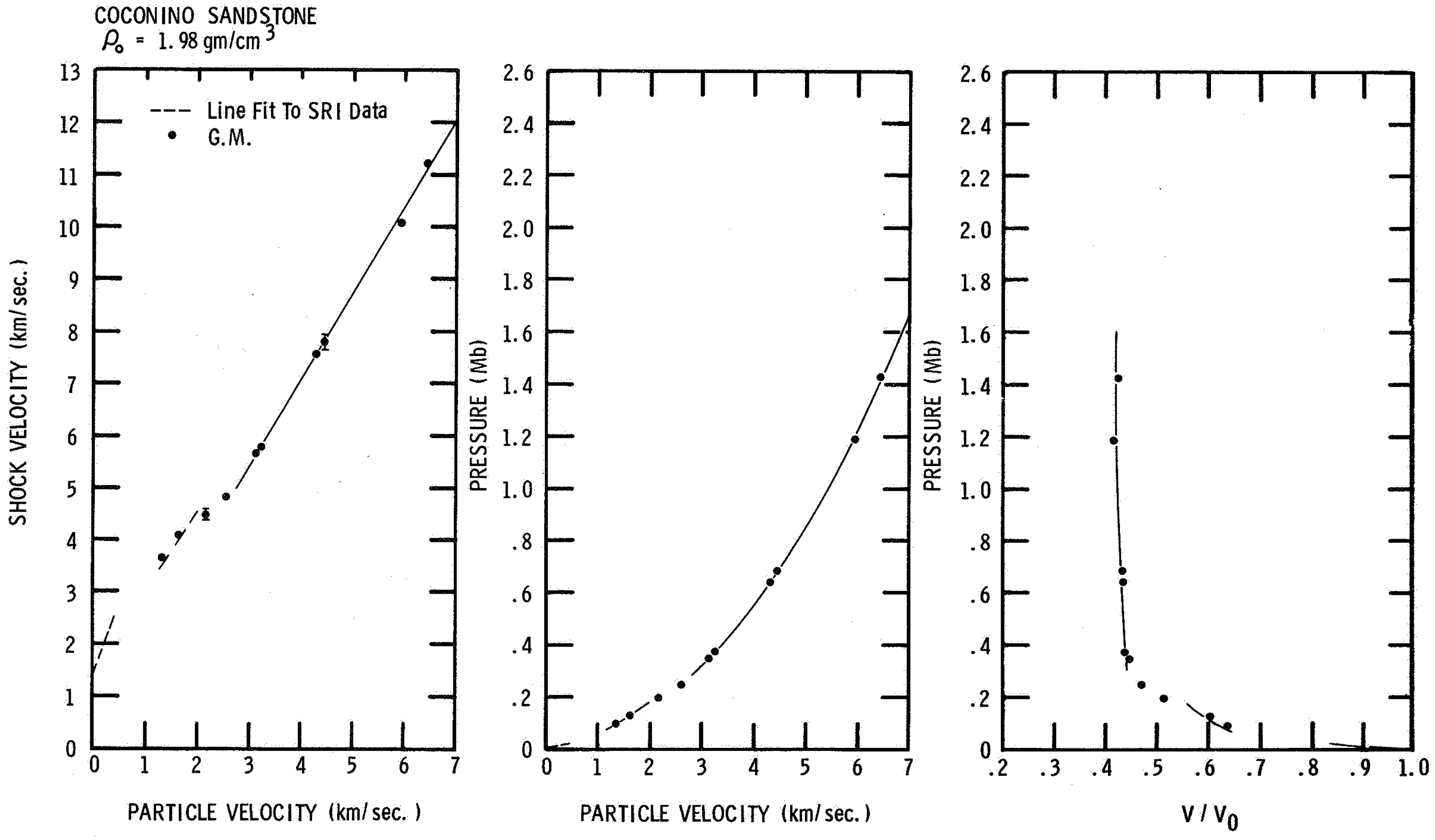

Figure 9 Hugoniot Data for Coconino Sandstone

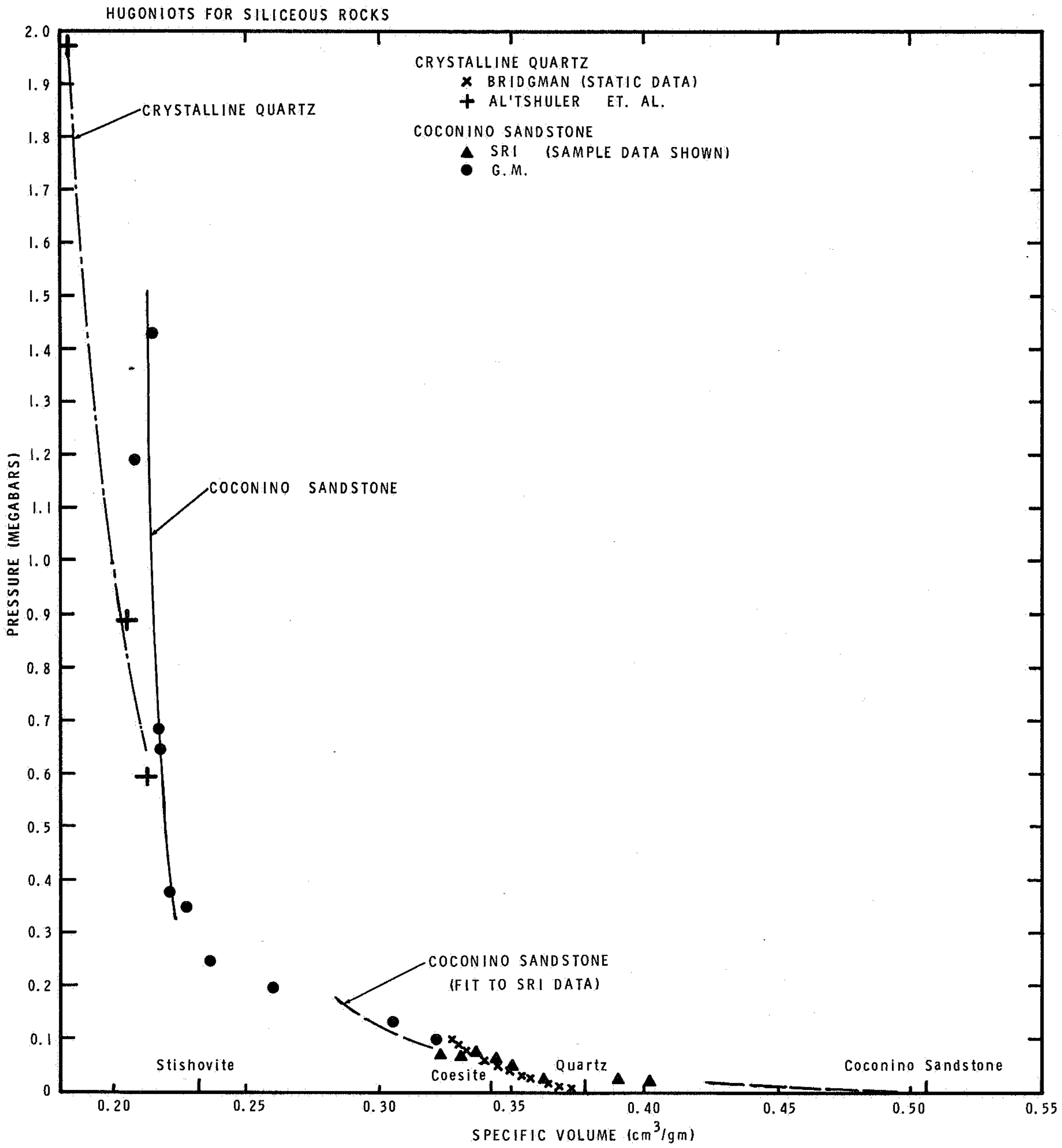

Figure 10 Hugoniot Data for Siliceous Rocks

change (region four) in the pressure range 0.15 Mb to 0.35 Mb. Based on the observed transition pressures and volume changes, it would appear that these two phase changes correspond to the transition of quartz to coesite and coesite to stishovite respectively. The second transition to stishovite is in good agreement with the observed transformation in solid quartz, which is assumed to be the quartz-stishovite phase change observed by Wackerle. There is deviation at higher pressures which is assumed to be the result of higher temperature achieved by the initially porous sandstone. Above this transition (the fifth region) the linear fit to the experimentally determined hugoniot points is given by

$$U_s = 0.36 + 1.67\ u_p \text{ km/sec}$$

Note that the data in Figures 9 and 10 show that single shocks exist in the coesite-stishovite mixed-phase region, indicating that the transition is neither complete nor sharp in the available time span.

Fused Quartz

Figure 11 presents the single hugoniot point obtained for fused quartz, together with the lower pressure data of Wackerle.(7) The large extrapolation of Wackerle's linear fit in the stishovite phase of quartz results in only a very small difference (~ 1.8% in shock velocity). This suggests, on the basis of a single point (and this must be emphasized), that no further phase change occurs in the fused quartz between 0.8 and 1.6 Mb.

Mono Crater Pumice

In the precursor study of Mono Crater pumice presented here, four hugoniot data points were measured for pressures from 0.03 to 0.3 Mb. Due to the extreme porosity of this material

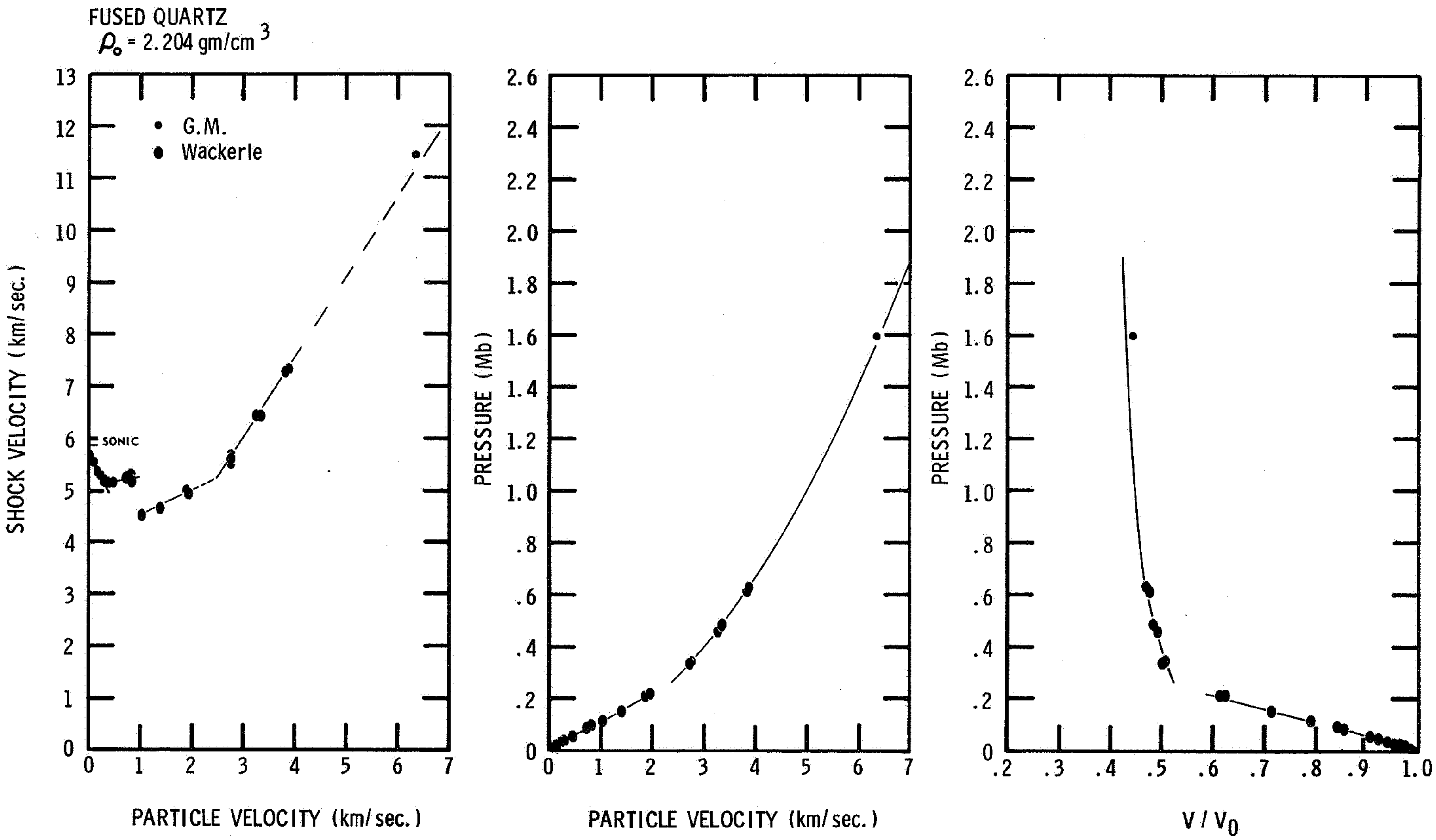

Figure 11 Hugoniot Data for Fused Quartz

(~ 78%) very high compressions are attained (~ 86% at 0.056 Mb) and the maximum compression is at a much lower pressure than in the sandstone. The accuracy of the data obtained is somewhat open to question, even though the individual data points do not show large scatter. For materials of large distensions, such as the pumice, the behavior of the induced shock wave is complex. Non-linear shock propagation has been found in other porous materials(8) which, for samples of the size tested here, may appear as decreasing shock velocity with increasing distance into the specimen. Since the measurement technique used yields only the average shock velocity through the specimen, the measurements are subject to question.

Tables VII and VIII list the physical properties and hugoniot data respectively. Figure 12 displays the hugoniot data for shock travel of 5.87 mm.

Zelux

Zelux is Westlake Plastics Company's trade name for stress relieved polycarbonate shapes produced from Lexan (registered trademark of the General Electric Company). The "M" designation sometimes attached to Zelux indicates a particular resin type. However, polycarbonate resins produce essentially identical Zelux, therefore, designation between the resins has little meaning. All Zelux produced from extruded rod or extruded and compression molded heavy sheet is annealed.

Tables IX and X list the physical properties and hugoniot data respectively. Figure 13 displays the hugoniot data graphically. A change of state apparently occurs at ~ 0.35 Mb. What the state of Zelux is beyond the phase change is at present not understood.

TABLE VII

PHYSICAL PROPERTIES OF MONO CRATER PUMICE

Chemical Composition

Source - U.S. Pumice Mine,
Lee Vining, California

SiO_2	75.7%
Al_2O_3	13.0%
Na_2O	4.0%
K_2O	4.5%
H_2O^+	0.71%
Fe_2O_3	0.626%
FeO	0.44%

Density

0.48 gm/cm^3 - 0.76 gm/cm^3

Porosity (calc)

78%

Grain Density (calc)

2.54 gm/cm^3

Vesicle Size = 1.5 x 1.5 x 4 mm to 0.02 x 0.02 x 0.27 mm

Vesicles are aligned parallel to the banding in the rock.

TABLE VIII

HUGONIOT DATA FOR MONO CRATER PUMICE

$\rho_o = 0.55\ gm/cm^3$

Us Shock Velocity (km/sec)	U_p Particle Velocity (km/sec)	P Pressure (Megabar)	V/V_o Relative Volume
2.77 ± .02	2.32	.035 ± .0002	.166 ± .003
3.45 ± .18	2.96	.056 ± .003	.144 ± .041
6.59 ± .16	5.31	.192 ± .005	.195 ± .018
7.81 ± .06	6.19 ± .20*	.266 ± .011	.208 ± .033

* Estimated Impact Velocity

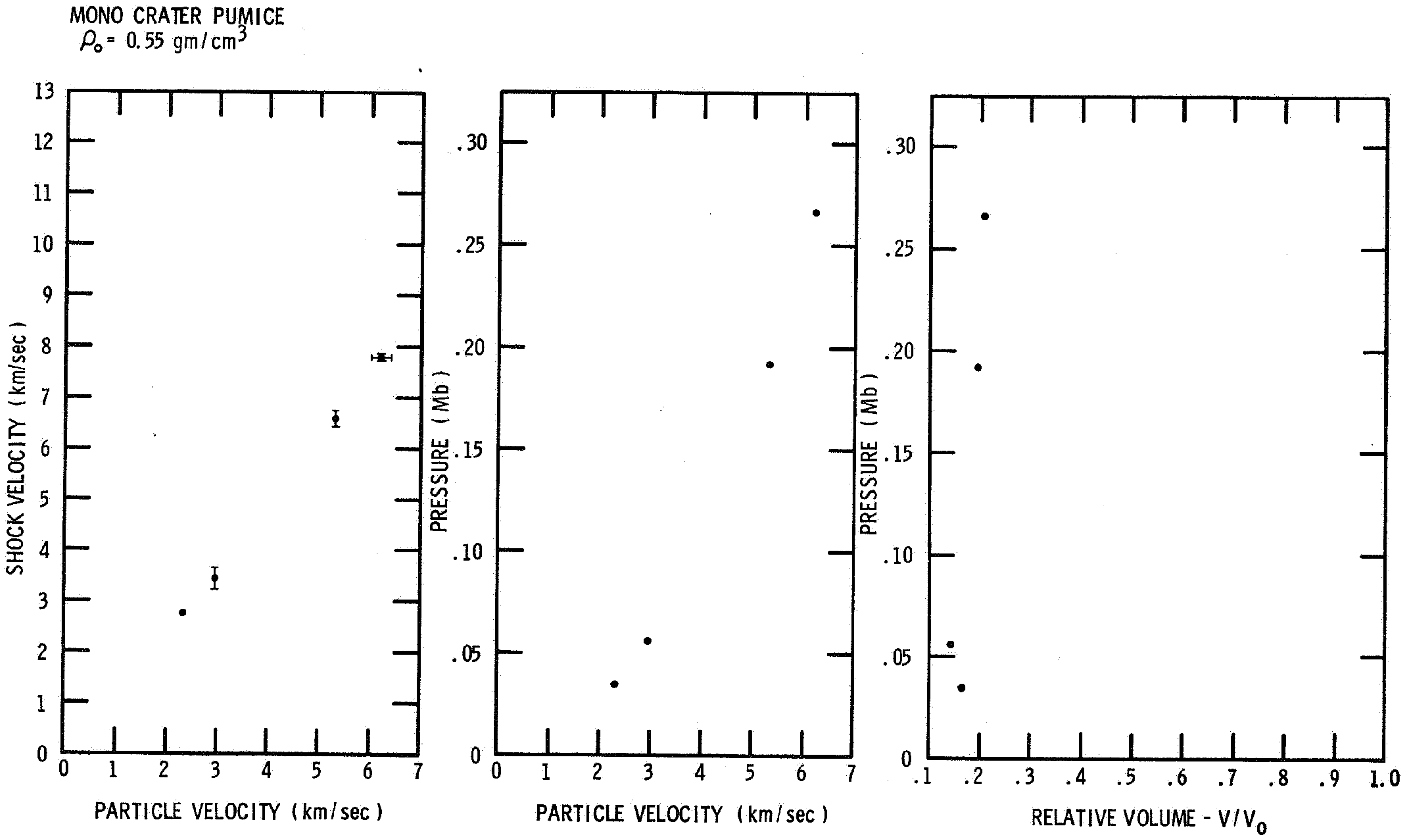

Figure 12 Hugoniot Data for Mono Crater Pumice

TABLE IX

PHYSICAL PROPERTIES OF ZELUX M

MECHANICAL PROPERTIES	
Tensile Strength, 10^8 dynes/cm^2	5.52 - 6.55
Compressive Strength, 10^8 dynes/cm^2	7.59
Impact Strength, Izod Ft lbs/in - Notch	12 - 16
Elongation, %	80 - 100
PHYSICAL PROPERTIES	
Density, gm/cm^3	1.20
Specific Volume, cm^3/gm	0.83
Machinability	excellent

TABLE X

HUGONIOT DATA FOR ZELUX

$\rho_o = 1.20$ gm/cm^3

U_s Shock Velocity (km/sec)	U_p Particle Velocity (km/sec)	P Pressure (Megabar)	V/V_o Relative Volume
5.82 ± .15	2.22	.155 ± .044	.619 ± .009
6.39 ± .005	2.81	.216 ± .001	.560 ± .004
6.96 ± .03	3.65	.305 ± .001	.476 ± .002
8.44 ± .05	4.72	.478 ± .003	.440 ± .004
9.83 ± .12	5.61 ± .20*	.662 ± .032	.430 ± .028
12.05+	6.92 ± .05*	1.001 ± .007	.426 ± .004

* Estimated Impact Velocity

\+ Single Pin Value

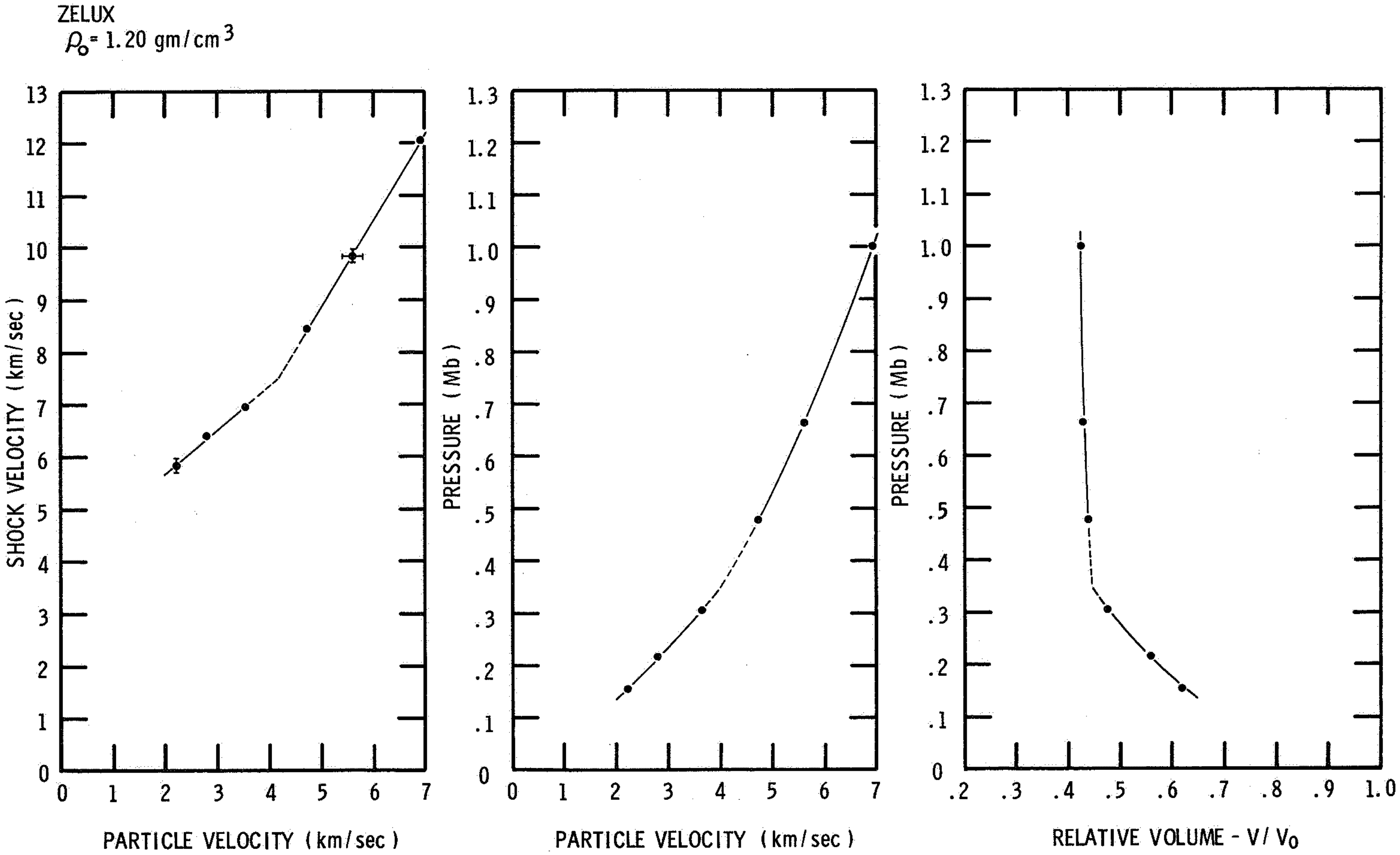

Figure 13   Hugoniot Data for Zelux

The linear fit to the data in the $U_s - u_p$ plane consists of two segments of the form:

$$U_{s1} = 4.11 + 0.789\ u_p \text{ km/sec for } 2.0 < u_p < 4.05 \text{ km/sec}$$

$$\text{Sigma } U_{s1} = \pm\ 0.09 \text{ km/sec}$$

and

$$U_{s2} = 0.65 + 1.645\ u_p \text{ km/sec for } 4.05 < u_p < 7.0 \text{ km/sec}$$

$$\text{Sigma } U_{s2} = \pm\ 0.06 \text{ km/sec}$$

Recovery Shots

The possibility of detecting a metastable phase of olivine gave rise to the idea of recovering shocked debris of Vacaville basalt. Two preliminary experiments were conducted for shock wave pressure of ~ 0.7 Mb. It became evident that a successful program would represent a formidable part of the present contract because of the problem of safeguarding the recovery material and catcher from damage by the high pressure hydrogen used to accelerate the projectile. For this reason, the recovery experiments were terminated.

TABLE XI

SUMMARY OF LINEAR EQUATION OF STATE PARAMETERS

Material	ρ_o gm/cm^3	Pressure Range Mb	C_o (km/sec)	S	Porosity %
Vacaville Basalt	2.86	0.3 - 2.1	2.306	1.615	< 2
Kaibab Limestone	2.22	0.3 - 1.1	1.891	1.597	20.3 - 23.8
Coconino Sandstone	1.98	0.07 - 0.2	1.43	1.56 (Ahrens)	25.8
		~0.3 - 1.5	0.36	1.67	
Mono Crater Pumice	0.55	0.03 - 0.27			78
Zelux	1.20	0.16 - .30	4.107	0.789	-
		0.30 - 1.0	0.648	1.645	-

SECTION III

HIGH STRAIN-RATE STUDIES

EXPERIMENTAL TECHNIQUES

The low and medium strain rates were obtained using an Instron screw driven testing machine and the General Motors developed Medium Strain-Rate Machine. The Medium Strain-Rate Machine shown in Figure 14 is similar in principle to those used by Clark and Wood(9) and Campbell and Marsh.(10) This machine is a completely gas-operated device with a lightweight movable piston capable of traveling in one direction for compression testing and in the other direction for tension testing. The piston velocity, and hence the rate of loading is controlled by the size of the discharge orifice (see Figure 14), the gas used, the pressure in the reservoirs, and to some extent, the test specimen. By proper selection of gas, pressure, and orifice size, the desired constant rate can be obtained for any specimen. The upper rate of the machine is not fixed, but depends on the accuracy required and the specimen material and geometry. An upper limit based on stress wave propagation might be as low as 10-20/second.

The load applied to the specimen is measured by strain gages mounted on an elastic load bar directly above the specimen. Specimen strain is obtained by measuring piston displacement, by using strain gages mounted on the specimen, or by use of an optical extensometer which tracks marks placed on the specimen. The brittle nature of the basalt under atmospheric conditions precluded the possibility of obtaining strain by measuring piston

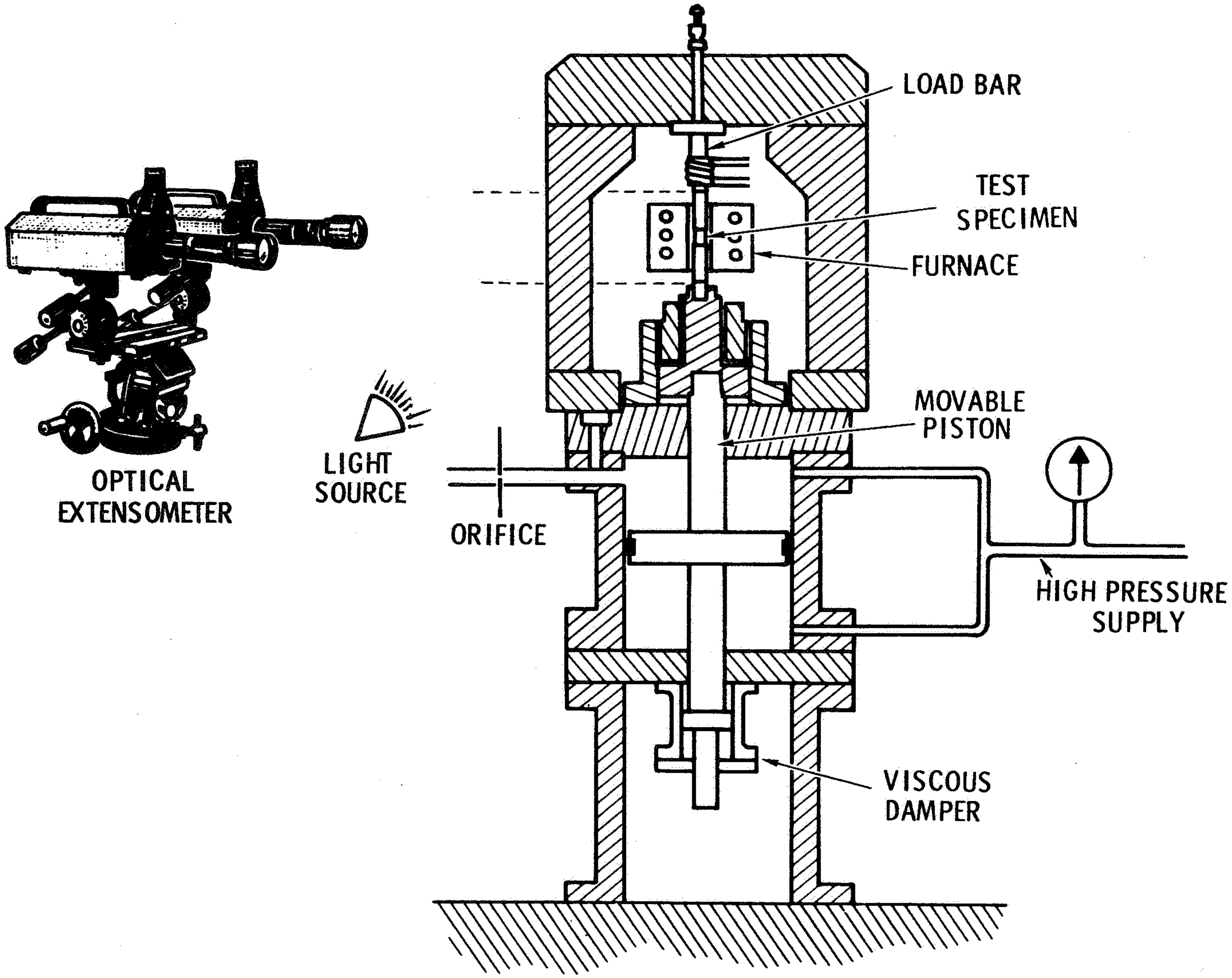

Figure 14 Schematic of Medium Strain-Rate Machine

displacement because the testing machine softness is of the same order as the specimen strain. Strain for the more ductile Zelux was obtained with the optical extensometer. A more complete description of the Medium Strain-Rate Machine is found in Reference 11.

The very high rate tests were performed on a split Hopkinson bar apparatus. This device has been used for high rate testing of metals by Kolsky(12), Campbell(13), and others.(14-19) The device is shown schematically in Figure 15. An elastic driver bar is accelerated down a launch tube by compressed air to impact an elastic weighbar, resulting in a stress wave passing down the weighbar. Part of the wave is reflected in the specimen-weighbar interface and part is transmitted through the specimen into the anvil bar. Strain gages mounted on the weighbar and anvil bar record the stress waves, which are analyzed to obtain a dynamic stress strain curve for the test material. The analysis requires that the theory of one-dimensional wave propagation holds. Reference 20 gives a complete description of the device as well as the data reduction methods.

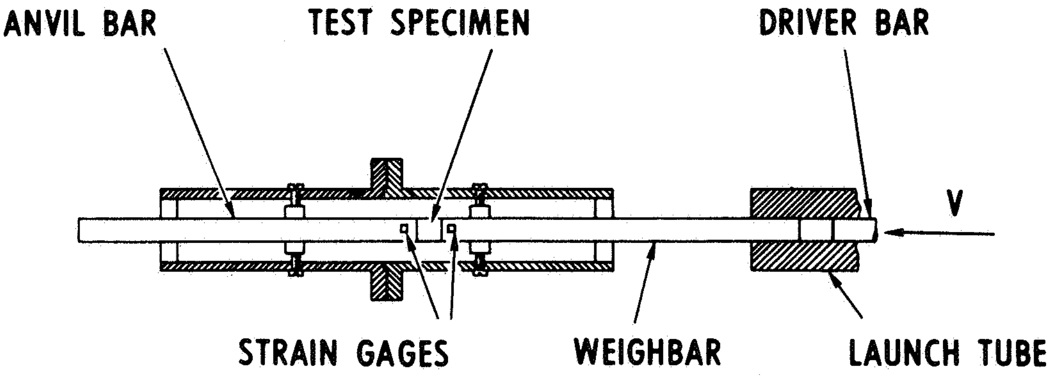

Figure 15 Schematic of Hopkinson Bar Device

EXPERIMENTAL RESULTS

Vacaville Basalt

The results obtained from uniaxial compressive stress tests conducted at constant strain rates from 10^{-5} to 10^{3}/second are shown in Figure 16. Basalt behaved in an elastic-brittle manner exhibiting increased fracture stress with increasing strain rates. Stiffness is independent of strain rate.

The stress-strain curve for basalt is composed of three distinct parts. The first is a non-linear region of increasing stiffness attributable to the filling of pores and microcracks as the initial stress is applied. Second, after the pores and microcracks have been filled, the approximately linear stress-strain relation reflects the reactions of the bulk rock supporting the load. Third, as the stress approaches the fracture stress of the material, the basalt exhibits increased non-linear behavior resulting from the nucleation of cracks.

The failure mechanism of the basalt rock under very high strain-rate compressive loading was investigated macroscopicly through photographic techniques. Pictures of basalt specimens under load in the split Hopkinson bar were obtained with a Polaroid camera using a very short duration (less than one microsecond) strobe light to provide illumination of the specimen as well as the shutter action of the camera. A photograph of the experimental arrangement is shown in Figure 17. The strobe light was synchronized to the test through the time delay circuit of the data recording oscilloscope. The coupling of the strobe light trigger to the oscilloscope made it possible

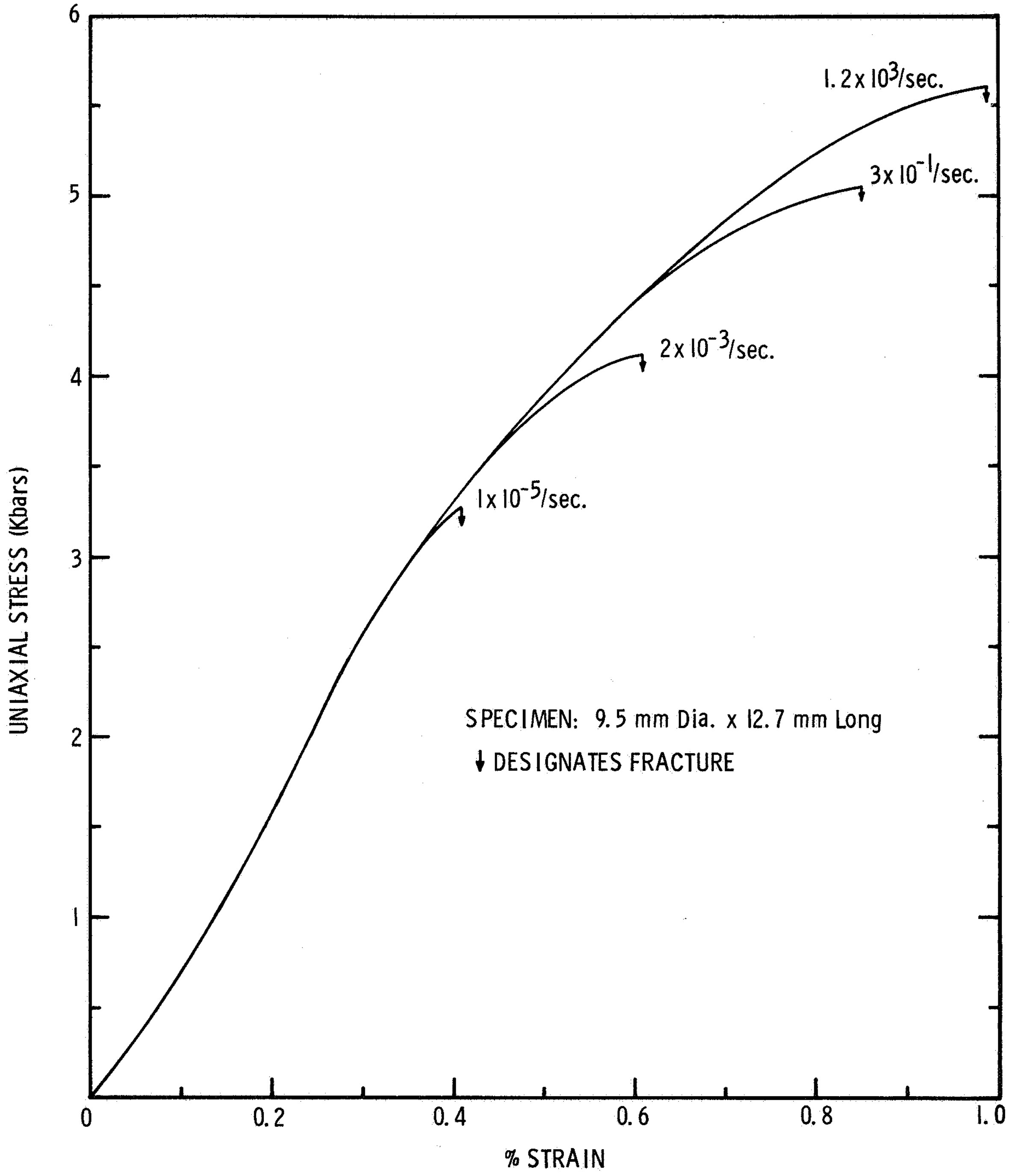

Figure 16 Uniaxial Compressive Stress-Strain Behavior of Basalt

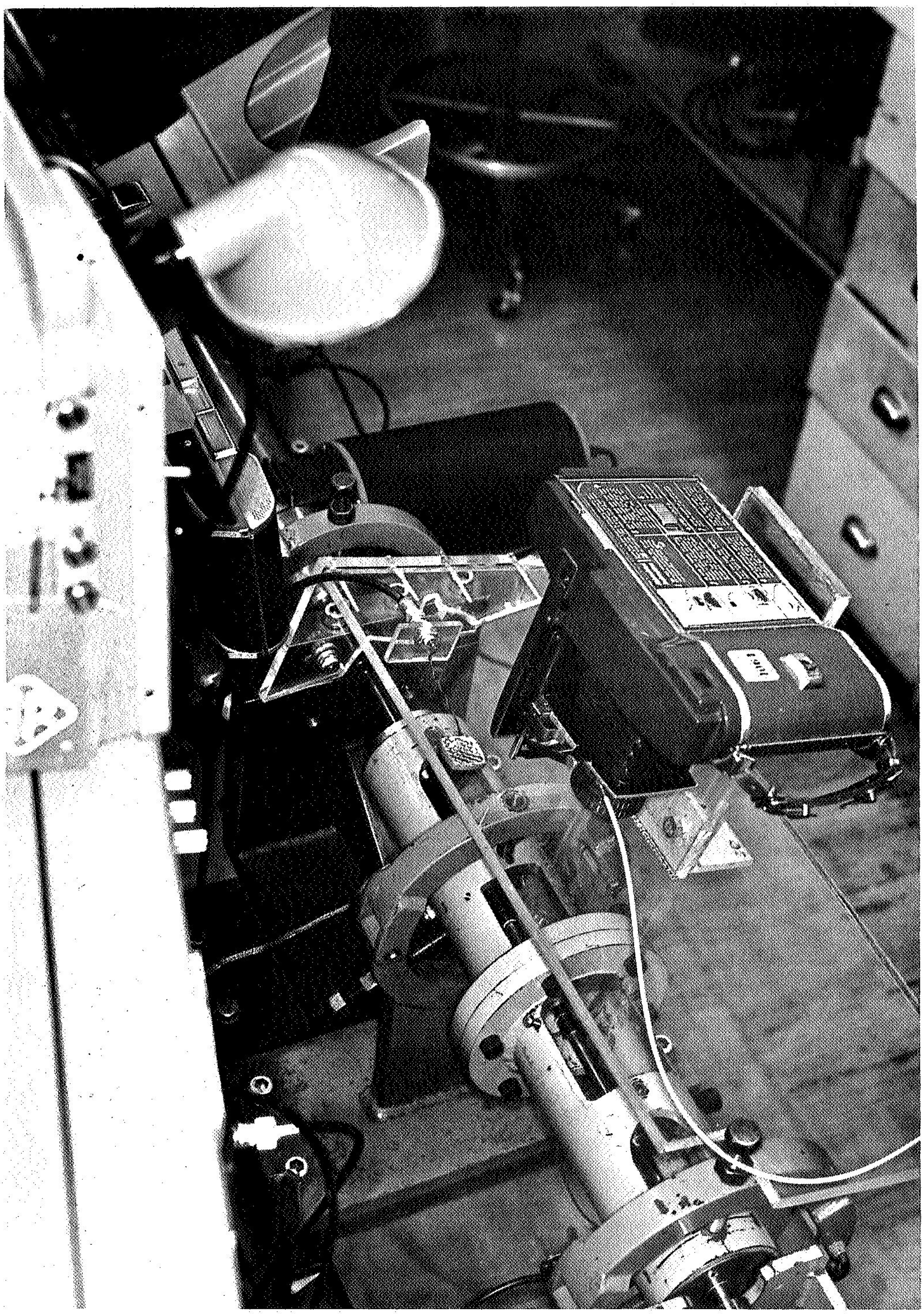

Figure 17 Hopkinson Bar Photographic Setup

to obtain pictures of the specimen at any time during the test. Figure 18 contains a series of pictures of the basalt under load. Each of the photographs was obtained during an individual test then compiled to form a series representative of one specimen during an average test.

Following the pictures in Figure 18, the specimen in the photograph labeled "Specimen Loaded to 98% of Fracture Stress" does not show any cracks. The first visible cracks in the specimens appear as the fracture stress is obtained. In the picture labeled "Specimen About 2 μsec After Fracture," a longitudinal crack may be seen in the center of the specimen. The remainder of the photographs in Figure 18 show specimens at various times after fracture. (The light colored areas seen at the faces of the test specimen are sprays of lubricating oil from the specimen-bar interfaces.) The pictures indicate that high strain-rate fracture is the result of nucleation and propagation of longitudinal cracks followed by outward slabbing of the dislocation fragments. The longitudinal cracks result from shear failure of the material, i.e., shear cones are formed at either end of the specimen which when further compressed into the material produce the longitudinal cracks visible in the photographs.

Figure 19 shows photomicrographs of typical specimens of the basalt rock tested here. The light colored "patches" in the photomicrographs are grains while the dark areas, which appear to be out of focus, are voids. The very small dark spots are inclusions. Careful high magnification examination of test specimens before loading revealed only a few microcracks and no large cracks. From these photographs, the grain diameter varies from about 0.01 to 0.10 mm.

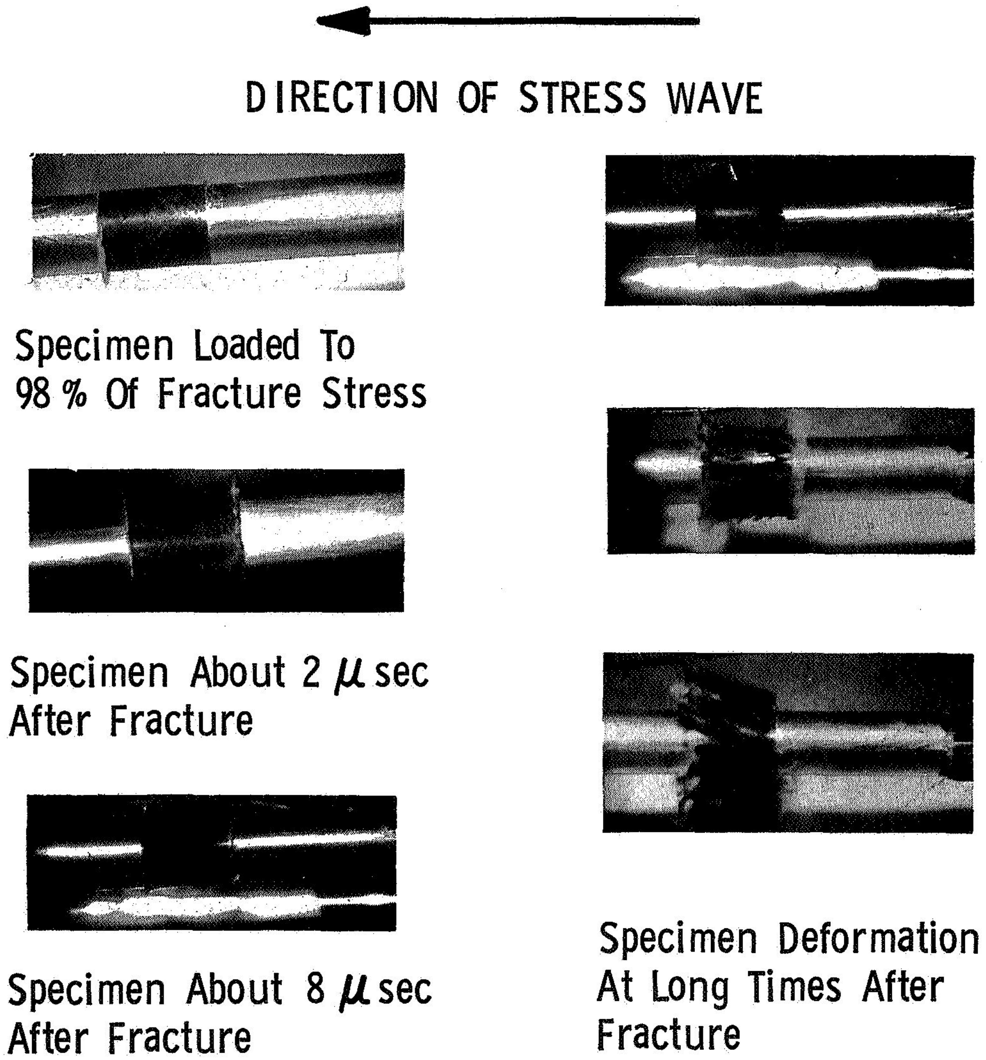

Specimen Loaded To
98 % Of Fracture Stress

Specimen About 2 μsec
After Fracture

Specimen About 8 μsec
After Fracture

Specimen Deformation
At Long Times After
Fracture

Figure 18 Photographs of High Strain-Rate Fracture of Basalt

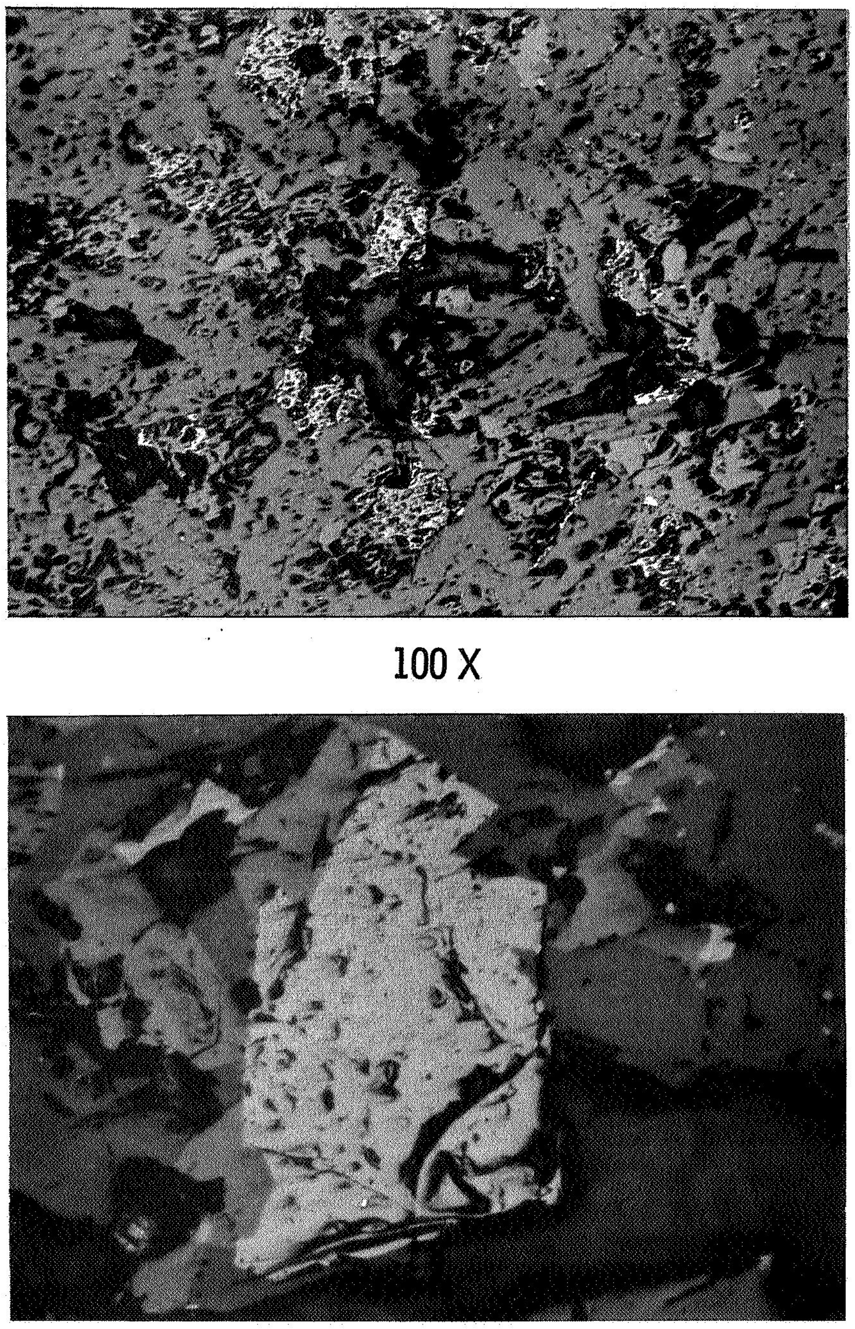

100 X

500 X

Figure 19 Photomicrographs of Basalt

Zelux

Results of the uniaxial stress investigation of Zelux as a function of strain rate are shown in Figure 20. Zelux exhibits a viscoelastic behavior over strain-rates from 10^{-4} to 10^{3}/second. This behavior is explained in that, at the low strain-rates, the polymer side groups have time to re-adjust and relax the stress; at the higher strain-rates, however, the side groups do not have time to re-adjust, consequently requiring a higher stress for a given strain. Yield stress occurred at approximately 8% strain independent of the strain rate. Zelux deforms ductily to large strains at all strain rates. A detailed discussion of the strain-rate sensitivity of various polymers may be found in Reference 21.

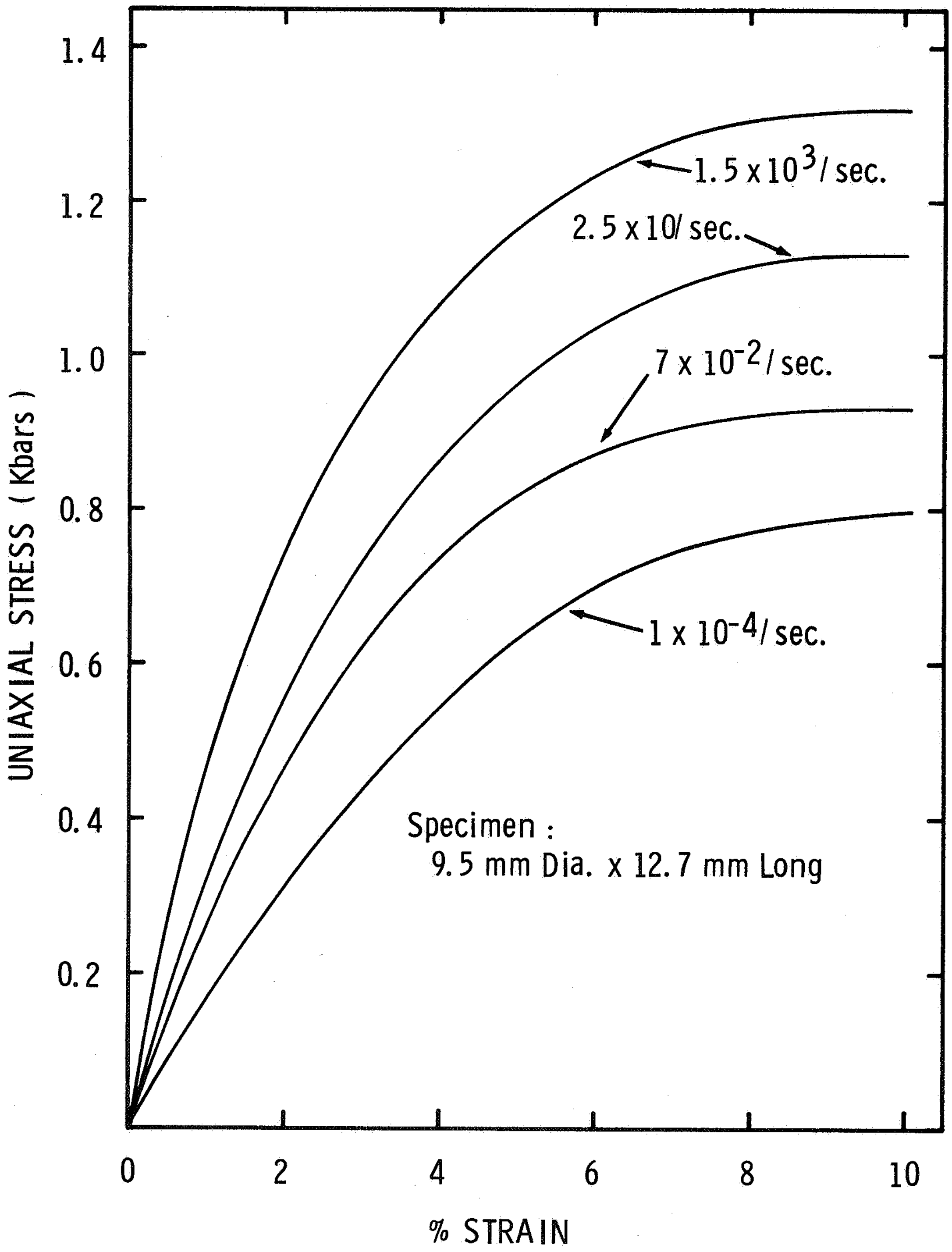

Figure 20 Uniaxial Compressive Stress-Strain Behavior of Zelux

SECTION IV

CONCLUSIONS

The experimental determinations of the hugoniot equations of state for Vacaville basalt, Kaibab limestone, Coconino sandstone and Mono Crater pumice are presented in this report. The following conclusions may be drawn from these data:

1. The hugoniots of Vacaville basalt and Kaibab limestone appear well-behaved, i.e. within the limits of experimental error there are no phase change discontinuities observed over the range of pressures achieved.

2. The hugoniot for Coconino sandstone exhibits two phase changes which are assumed to be the quartz-coesite and coesite-stishovite transition.

3. The single data point on the hugoniot of fused quartz suggests that no further phase changes take place between 0.80 and 1.6 Mb.

No conclusion is presented for the Mono Crater pumice because unsufficient experimental data has been gathered.

The additional testing of the polycarbonate resin, Zelux, resulted in the determination of its hugoniot equation of state.

4. The hugoniot of Zelux was found to exhibit a phase change at ~ 0.35 Mb.

The high strain-rate experimental results are summarized by the following conclusions:

1. Vacaville basalt under uniaxial compressive stress was found to exhibit increasing fracture stress with strain rates increasing from 10^{-5}/sec to 10^{3}/sec. The stress-strain behavior of this material was elastic-brittle with failure occurring through shear.

2. Zelux displayed viscoelastic behavior when tested in uniaxial compressive stress at various strain rates. The yield stress of this material occurred at approximately 8% strain independent of the strain rate. Large ductile compression was possible even at the highest strain rates.

SECTION V

REFERENCES

1. Al'tshuler, L.V.,"Use of Shock Waves in High Pressure Physics", Sov. Phys. USPEKHI, 8, 52 (1965)

2. Curtis, J.S. "An Accelerated Reservoir Light-Gas Gun", NASA TN D-1144, 1962

3. Walsh, J.M., et al., Phys. Rev., 108, 196 (1957)

4. Ahrens, T.J., et al., "Shock Compression of Crustal Rocks: Data for Quartz, Calcite and Plagioclase Rocks", J. Geophys. Rev., 69, 4839 (1964)

5. Bass, R.C., et al., "Hugoniot Data for Some Geological Materials", Sandia Corporation, Albuquerque, N.M., SC-4903 (RR), June 1963.

6. Lombard, D.B., "The Hugoniot Equation of State of Rocks", Lawrence Radiation Laboratory, University of California, USRL-6311

7. Wackerle, J. H., "Shock-Wave Compression of Quartz", J. Appl. Phys., 33, 922 (1962).

8. Butcher, B.M., "Dynamic Crushup of Foams", Sandia Laboratory, Albuquerque, N.M., SC-RR-66-325, May, 1967

9. Clark, D.S. and Wood, D.S., "The Time Delay for the Initiation of Plastic Deformation at Rapidly Applied Constant Stress", Proc. of the ASTM, Vol. 49, 1949

10. Campbell, J.D. and Marsh, K.J., "The Effect of Grain Size on the Delayed Yielding of Mild Steel", Philosophical Mag., Vol. 7, No. 78, June 1962

11. Babcock, S.G., Kumar, A., and Green, S.J., "High Strain Rate Properties of Eleven Reentry-Vehicle Materials at Elevated Temperatures", AFFDL TR-67-35, Part I, April, 1967

12. Kolsky, H., "An Investigation of the Mechanical Properties of Materials at Very High Rates of Loading", Proc. of the Physical Soc., Vol. 62, 1949

13. Campbell, J.D. and Duby, J., "The Yield Behavior of Mild Steel in Dynamic Compression", Proc. of the Royal Society A, Vol. 236, 1956

14. Krafft, J. M., Sullivan, A.M. and Tipper, C.F., "The Effect of Static and Dynamic Loading and Temperature on the Yield Stress of Iron and Mild Steel in Compression", Proc. of the Royal Society A, Vol. 221, 1954

15. Maiden, C.J. and Campbell, J.D., "The Effect of Impact Loading on the Static Yield Strength of a Medium-Carbon Steel", Philosophical Mag., Vol. 3, 1958; also Maiden, C.J., "The Strain Rate Sensitivity of α-Uranium", J. Mech. Phys. Solids, Vol. 7, 1959

16. Hauser, F.E., Simmons, J.A. and Dorn, J.E., "Strain Rate Effects in Plastic Wave Propagation", Proc. of Met. Society Conferences, Vol. 9, 1960

17. Davies, E.D.H. and Hunter, S.C., "The Dynamic Compression Testing of Solids by the Method of the Split Hopkinson Bar", J. Mech. Phys. Solids, Vol. 11, 1963

18. Chiddister, J.L. and Malvern, L.E., "Compression-Impact Testing of Aluminum at Elevated Temperatures", Experimental Mechanics, Vol. 3, 1963

19. Karnes, C.H. and Ripperger, E.A., "Strain Rate Effect in Cold Worked High-Purity Aluminum", J. Mech. Physics Solids, Vol. XIV, 1966

20. Maiden, C.J. and Green, S.J., "Compressive Strain Rate Tests on Six Selected Materials at Strain Rates from 10^{-3} to 10^4 in./in./sec.", J. Appl. Mech., Vol. 33, Sept. 1966

21. Kumar, A., Perkins, R.D. and Schierloh, F.L., "Dynamic Behavior of Polymers and Composites", SAMSO TR-68-71, Vol. 5 and GM Manufacturing Development, MSL-68-8, February, 1968.

(Reverse Page is blank)